

ASSESSING EOLIAN DUST INPUTS TO SOILS
IN DRY CREEK EXPERIMENTAL WATERSHED, SW IDAHO

by

Brian Jameson Stark

A thesis

submitted in partial fulfillment

of the requirements for the degree of

Master of Science in Hydrologic Sciences

Boise State University

December 2012

© 2012

Brian Jameson Stark

ALL RIGHTS RESERVED

BOISE STATE UNIVERSITY GRADUATE COLLEGE

DEFENSE COMMITTEE AND FINAL READING APPROVALS

of the thesis submitted by

Brian Jameson Stark

Thesis Title: Assessing Eolian Dust Inputs to Soils in Dry Creek Experimental Watershed, SW Idaho

Date of Final Oral Examination: 14 September 2012

The following individuals read and discussed the thesis submitted by student Brian Jameson Stark, and they evaluated his presentation and response to questions during the final oral examination. They found that the student passed the final oral examination.

Shawn G. Benner, Ph.D.	Chair, Supervisory Committee
Jennifer L. Pierce, Ph.D.	Member, Supervisory Committee
James P. McNamara, Ph.D.	Member, Supervisory Committee
Paul H. Olin, Ph.D.	Member, Supervisory Committee

The final reading approval of the thesis was granted by Shawn G. Benner, Ph.D., Chair of the Supervisory Committee. The thesis was approved for the Graduate College by John R. Pelton, Ph.D., Dean of the Graduate College.

ACKNOWLEDGEMENTS

The author wishes to express gratitude to those who have helped make this thesis possible. Thank you to the National Science Foundation and the Boise State University Department of Geosciences for their generous support. Thank you to Dr. Shawn Benner, Dr. Jen Pierce, Dr. Jim McNamara, and Dr. Paul Olin for serving on my supervisory committee. Thank you to Dr. Karen Viskupic, Dr. David Wilkins, and Dr. Jim Belthoff for giving me the opportunity for personal growth through Boise State's GK-12 project, and to Sara Focht and Dave Cannamela for helping me to achieve that growth. Thank you to Mike Poulos for being my partner in the field and Dr. Paul Olin for numerous lab consultations. Finally, special thanks to Dr. Shawn Benner for mentoring me throughout this thesis and to my wife, Astrid Stark, for her tireless support and encouragement.

ABSTRACT

A geochemical investigation of upland soils in the Dry Creek Experimental Watershed (DCEW) near Boise, Idaho was conducted to assess the potential contributions of eolian dust. Major and trace element compositions of soils within the watershed, loess deposits in the adjacent Western Snake River Plain (WSRP), and underlying granodiorite bedrock were evaluated. Multiple lines of evidence suggest a significant contribution of dust in the soils. Plots of Co/Ti, V/Ti and Cr/Ti indicate that the loess and bedrock occupy distinctly different compositional spaces and that the soils are of intermediate composition, suggesting that the soils are a mixture of the loess and bedrock. In the same compositional space, isolates of the silt + clay size fraction exhibit compositions closer to the loess field than the associated bulk soils, also consistent with a dust contribution. A two-component mixing model, using the granodiorite and loess as end-members, indicates there is an average of 28% dust in the soils. This model also indicates that the dust contribution is greater in the upper portions of soil profiles, and that the dust contribution on north facing slopes is more than double that on south facing slopes (38% and 16%, respectively). Dust appears to be the dominant contributor of fine-grained material to these soils. Theoretical removal of estimated dust contributions from DCEW soils reduced soil water storage capacity by an average of 48% in the soils, suggesting that dust deposition is an important contributor to shallow water storage capacity and subsequent summertime availability in the upland soils of this watershed.

TABLE OF CONTENTS

ACKNOWLEDGEMENTS.....	iv
ABSTRACT.....	v
LIST OF TABLES.....	ix
LIST OF FIGURES.....	x
1 INTRODUCTION.....	1
1.1 Problem Statement.....	1
1.2 Loess.....	2
1.3 Study Area.....	4
1.4 Geology.....	5
1.5 Hydrology.....	7
1.6 Hypothesis Statement.....	8
2 METHODS.....	11
2.1 Site Selection.....	11
2.2 Sample Collection.....	12
2.2.1 Collection of Soil Samples.....	12
2.2.2 Collection of Loess Samples.....	13
2.2.3 Collection of Bedrock Samples.....	13
2.2.4 Collection of Basalt Samples.....	14
2.3 Sample Preparation.....	14

2.3.1 Whole Rock and Soil Fusions.....	14
2.3.2 Acid Digestions.....	17
2.4 Estimating Loess Fractions in Soils Using a Two-Component Mixing Model....	17
2.4.1 Two-Component End-Member Mixing Model.....	17
2.4.2 Criteria for Mixing Model Inputs	18
2.4.3 Mixing Model Assumptions	19
2.5 Determination of Sample Variability.....	20
3 RESULTS	21
3.1 Loess Composition.....	21
3.1.1 Major Elements.....	21
3.1.2 Trace Elements.....	21
3.1.3 Rare Earth Elements	22
3.1.4 Dust in the Snowpack	22
3.2 Bedrock Composition	23
3.3 Soil Composition	24
3.3.1 Comparison of Soils to End-Members.....	24
3.3.2 Isolated Grain-Size Fractions.....	26
3.4 Local Basalt Composition.....	27
3.5 Chemical Loess Fraction Estimates	28
4 DISCUSSION	29
4.1 Evaluation of Predicted Trends.....	29
4.1.1 Soils as a Product of Mixing.....	29
4.1.2 Grain-Size Distribution.....	30

4.1.3 Soil Fine Fractions	31
4.1.4 Elevation	32
4.1.5 Soil Depth	33
4.1.6 Slope Aspect	34
4.2 Other Possible Explanations for DCEW Soil Characteristics.....	35
4.2.1 Weathering of Bedrock	35
4.2.2 Basalt Influences	37
4.2.3 Other Influences.....	39
4.3 Ecohydrological Implications of Loess Inputs to Dry Creek Soils.....	41
4.4 Suggestions for Future Work	44
CONCLUSIONS.....	46
REFERENCES	47
APPENDIX.....	79
BSU Isotope Geology Laboratory – Clean Lab Procedures	79

LIST OF TABLES

Table 1:	Major element data (ICP-MS) for all bulk samples.....	54
Table 2:	Minor and trace element data (ICP-MS) for all bulk samples.....	55
Table 3:	Rare earth element data (ICP-MS) for all bulk samples.....	56
Table 4:	Chemical loess fraction estimates for Dry Creek soils.....	57
Table 5:	Chemical loess fraction versus elevation.....	58
Table 6:	Summary of the no-dust scenario exercise.....	58

LIST OF FIGURES

Figure 1:	Map of the study area.....	59
Figure 2:	Elemental concentrations in average bedrock, average loess, selected bulk soil MLN, 0-10 cm depth), and associated soil fine fractions (<75µm)...	60
Figure 3:	Major element composition of the WSRP loess.	61
Figure 4:	Trace element composition of WSRP loess.....	62
Figure 5:	Rare Earth element composition of WSRP loess.....	63
Figure 6:	Select trace element compositions of snowpack dust in the DCEW.	64
Figure 7:	Major element composition of DCEW bedrock.	65
Figure 8:	Major element comparisons of DCEW soil to loess and bedrock.	66
Figure 9:	Trace element comparison of DCEW soils to loess and bedrock.....	67
Figure 10:	Trace element comparison of DCEW soil classes.....	68
Figure 11:	Rare Earth element patterns of DCEW soils, WSRP loess, DCEW bedrock, and local basalt.....	69
Figure 12:	Comparison of trace element concentrations in grain size isolates of selected soil (HS site, 0-10 cm depth).	70
Figure 13:	Major element composition of local basalt.....	71
Figure 14:	Comparison of grain size distribution curves of saprolites, loess and selected soils.	72
Figure 15:	Percent increase in silt content in DCEW soils relative to saprolites.	73
Figure 16:	Chemical loess fractions for all soils as a function of soil depth.....	74
Figure 17:	Chemical loess fractions as a function of slope aspect.	75

Figure 18: Trace element comparison of local basalt to DCEW bedrock, DCEW soils, and WSRP loess..... 76

Figure 19: Uranium versus titanium concentrations of local basalt..... 77

Figure 20: Comparison of chemical loess fractions to existing silt + clay content at Dry Creek soil sites..... 78

1 INTRODUCTION

1.1 Problem Statement

The grain-size characteristics and thickness of soils control hydrologic properties and, in some cases, dramatically influence associated vegetative communities of watersheds (Brady and Weil, 1999; Laio *et al.*, 2001; Rodriguez-Iturbe *et al.*, 2001). In the Dry Creek Experimental Watershed, strong gradients in soil depth (Tesfa *et al.*, 2009) and soil texture (Smith *et al.*, 2011; Geroy *et al.*, 2011) with topography, elevation, slope aspect, and morphology (Nicótina *et al.*, 2011; Poulos *et al.*, 2012) are accompanied by dramatic variations in vegetative patterns (McNamara *et al.*, 2005; Williams, 2005) and associated differences in soil and above-ground carbon reservoir sizes (Smith, 2010; Kunkel *et al.*, 2011). The variations attributable to a complex interplay between climatic and geomorphologic drivers and feedbacks including temperature, precipitation amount and type, insolation, evapotranspiration, and erosional and depositional processes have apparently strongly influenced geomorphological evolution of the landscape (Poulos *et al.*, 2012). It is generally accepted that all of the factors listed above influence pedogenic processes, however the relative importance of any one factor is difficult to constrain due to the complexity of feedbacks and spatio-temporal variation in the factors at even modest regional scales. Observations of thicker, finer soils on north aspects where there is more diverse and abundant vegetation, higher silt content in soils than one would expect in soils derived from crystalline rock (Kwon and Oh, 2011), and close proximity

of loess deposits in the adjacent Snake River Plain suggest that deposition of dust may be an important influence on soil pedogenesis in this system. These deposits may influence vegetation development and climate-vegetation-geomorphology interactions. This study focused on eolian deposition as an important contributor of fine grained material to these soils, potentially influencing the hydrology, ecological function, and geomorphology of this landscape.

Numerous studies have demonstrated the importance of eolian inputs to regolith in the western United States (Lawrence *et al.*, 2011; Chadwick and Davis, 1990; Dahms, 1993; Goldstein *et al.*, 2008; Reheis and Kihl, 1995; Reynolds *et al.*, 2006; Ferrier *et al.*, 2011). Within that framework, recognition of eolian contribution to soils in the Dry Creek Experimental Watershed would provide further documentation that this process is important in the region, and perhaps exert a controlling influence on soil formation in the watershed.

1.2 Loess

Loess is regarded by most researchers as a distinct body of accumulated eolian sediment (Muhs, 2007; Pye, 1987; Muhs and Bettis, 2004). Loess deposits are characterized by primarily silt-sized sediment (2-50 μm), but often contain some sand and clay (Muhs, 2007; Lewis *et al.*, 1975). Because wind-blown sediment (referred to as dust herein) is often derived from numerous sources, it typically has a chemical composition representative of the average upper continental crust (Gallet *et al.*, 1998). Common sources of dust include post-glacial outwash sediments (Smalley, 1966) and playa lake deposits and alluvium (Gillette *et al.*, 1980; Reheis and Kihl, 1995), but any

area of active erosion may contribute dust to downwind locations. Annually, 1700 Tg of dust is removed from terrestrial sources by wind (Jickells *et al.*, 2005) and it is estimated that 1250 Tg falls back onto land while 450 Tg falls into the oceans (Jickells *et al.*, 2005). If that 1250 Tg were evenly distributed across all continents, the rate of deposition would be approximately $8 \text{ t km}^{-2} \text{ yr}^{-1}$, which is significant when compared to the average global denudation rate of $140 \text{ t km}^{-2} \text{ yr}^{-1}$ (Wilkinson and McElroy, 2007; Ferrier *et al.*, 2011). Some areas are more proximal to dust sources and more conducive to deposition of suspended dust, which further differentiates how dust is redistributed across the landscape. The Loess Plateau in China is well known for thick (approximately 160 m) and well preserved accumulations (Muhs, 2007; Rutter *et al.*, 1996). In the US, thick accumulations of loess are present in the Great Plains, southeastern Washington, Alaska, Idaho, and Wyoming (Muhs, 2007; Lewis *et al.*, 1975; Pierce *et al.*, 1982; Sweeney *et al.*, 2004; Sweeney *et al.*, 2007; Pierce *et al.*, 2011; Dahms and Rawlins, 1996), serving as the medium for soil development in those areas. The airborne mechanism by which these fine-grained sediments are transported suggests that dust distribution is not limited to areas in which these ‘classic’ thick loess deposits are observable, rather deposition is widespread and commonly contributes to soils (Ferrier *et al.*, 2011; Lawrence *et al.*, 2011; Chadwick and Davis, 1990; Dahms, 1993; Goldstein *et al.*, 2008; Reheis and Kihl, 1995; Reynolds *et al.*, 2006; Yaalon and Ganor, 1973).

The addition of dust may significantly alter the grain-size distribution of soils, potentially influencing their moisture-holding capacity (Brady and Weil, 1999). Semi-arid ecosystems are characterized by extensive dry periods, which control the input of

water to soils. In upland semi-arid catchments, water available for biological function is often limited to water stored as soil moisture (Rodriguez-Iturbe *et al.*, 2001; McNamara *et al.*, 2005; Smith *et al.*, 2011). Soil water storage capacity is a function of both soil texture and soil depth. The addition of dust to soils adds mass (and possibly depth) to the soil profile, potentially providing increased storage volume relative to non dust-influenced soils.

1.3 Study Area

The study area is located in the Western Snake River Plain (WSRP) geologic province and adjacent foothills of the Boise Front Range near Boise, Idaho (Figure 1). The Dry Creek Experimental Watershed (DCEW) is located in the Boise Front Range, just to the northeast of Boise, Idaho. The 27 km² basin drains the headwaters of Dry Creek and spans an elevation gradient from 1100 m to 2100 m (Williams, 2005; McNamara *et al.*, 2005). The DCEW trends southwest-northeast and is dissected by several tributaries to Dry Creek that form a series of east-west trending ridgelines with asymmetric north and south facing slopes.

The DCEW is in a semi-arid climate that is characterized by cold, wet winters and hot, dry summers. Average annual precipitation is approximately 400 mm and 700 mm at low and high elevations, respectively, while air temperatures range from -15°C to 33°C and -14°C to 26°C in lower and upper elevations, respectively (McNamara *et al.*, 2005; Smith, 2010). The majority of precipitation falls as snow during the winter months in the upper watershed and temperatures support a seasonal snowpack. Winter precipitation occurs as rain and snow in the lower watershed and snow cover generally is not sustained

throughout the winter. Spring rain is common in the area, while summers have very little precipitation.

The USDA taxonomic classifications for soils in DCEW range from mesic Ultic Argixerolls in the lowlands to frigid Ultic Haploxerolls in the highlands (USDA, 2002). Soils are coarse, typically shallow (1-3m) with very low clay content (typically less than 10%), and exhibit loam, sandy loam, or loamy sand textures (Smith, 2010). Soils on north aspects are typically deeper than those on south aspects (Tesfa *et al.*, 2009).

There is distinct spatial differentiation of vegetation in the DCEW. At lower elevations in DCEW, south slopes are dominated by grasses, while north slopes can have a mixture of grasses, brush, and shrubbery. At mid elevations, the difference is more distinct with the occurrence of Douglas fir and pine species on north slopes and predominately grasses on south slopes. At upper elevations, conifers dominate both north and south slopes.

1.4 Geology

The WSRP is a southeast-northwest trending normal-fault bounded basin (Wood and Clemens, 2002). The 300 km long by 70 km wide basin is situated between the southern boundary of the Atlanta lobe of the Idaho batholith to the north, and smaller outlying granitic plutons of the Owyhee Mountains to the south. The graben basement is composed of a thick basaltic unit (Wood and Clemens, 2002). Overlying the basement rocks is a complex stratigraphy of mid-Miocene and younger basin fill, deposited during fluctuating levels of Lake Idaho coupled with bimodal rhyolitic and basaltic volcanic activity (Wood and Clemens, 2002). These units are predominately massive mudstones,

but are inter-bedded with some siltstones, sandstones, rhyolite and basalt flows, ash beds, poorly sorted alluvium, and variable deltaic deposits, particularly closer to the basin margins (Wood and Clemens, 2002; Wood, 1994). The massive mudstones are overlain by fluvial sands and gravels, predominately derived from the upland Idaho batholith (Othberg and Gillerman, 1994). The majority of the WSRP is mantled by loess with thicknesses ranging from less than 1 m to 6 m (Othberg and Stanford, 1992; Othberg *et al.*, 1997). Modern soils in the WSRP are derived primarily from loess parent material and exhibit calcic horizons or duripans at variable depths (Othberg *et al.*, 1997).

The northwestern edge of the WSRP is bound by the southern Atlanta lobe of the Cretaceous Idaho batholith (Clemens and Wood, 1993; Johnson *et al.*, 1988). The Atlanta lobe spans the majority of central Idaho, extending 275 km from north to south and 130 km from east to west (Othberg and Gillerman, 1994; Johnson *et al.*, 1988). The Atlanta lobe is comprised of six major rock types, but is primarily biotite granodiorite, which is mineralogically dominated by quartz and plagioclase feldspars, with 2-8 percent biotite (Johnson *et al.*, 1988). Biotite granodiorite outcrops are prevalent in the higher elevations of the Boise Front Range (Othberg and Gillerman, 1994). In the Boise Front Range, the Idaho batholith serves as the basement rock for mid-Miocene and younger Lake Idaho deposits and volcanic flows that were described in the previous section (Othberg and Gillerman, 1994). Lacustrine shore deposits of ancestral Lake Idaho are consistently but discontinuously present in the Boise Front up to an elevation of 975m, and reach a maximum elevation of 1128 m, suggesting the lake reached a maximum elevation of 1000 ± 130 m (Wood, 1994; Gallegos *et al.*, 1987). The Boise foothills are extensively

faulted along northwest-southeast striking faults parallel to the orientation of the WSRP (Othberg and Stanford, 1992). The granodiorite basement rock exhibits substantial fracturing (Wood and Burnham, 1987). Eocene dikes of both mafic and felsic composition are commonly found throughout the area (Clemens and Wood, 1993; Othberg and Gillerman, 1994). The basement rock in the Boise Front Range can be locally highly weathered, and, in places, leached as a result of geothermal activity (Wood, 1983).

1.5 Hydrology

The shallow hydrologic regime of the upland DCEW is characterized by McNamara *et al.* (2005). Soil-dry conditions in the summer transition to field capacity during the fall, as moisture input increases, temperature and insolation decrease, and plants enter dormancy. This is followed by a period in the winter when soil moisture is generally near field capacity as precipitation input to the soils are slow because the majority of precipitation falls as snow. In the spring, warmer temperatures melt the snowpack and common spring rains create a substantial influx of moisture to the soils, and field capacity is exceeded throughout the soil profile. It is during this period that precipitation, soil moisture, and lateral subsurface flow are truly connected, which is reflected by immediate stream flow response to precipitation inputs. This period is followed by late spring drying as evapotranspiration outpaces precipitation inputs, and the soils again fall below field capacity.

Spatial variations in soil moisture states in the watershed are controlled by snow distribution, hill slope position, and soil characteristics (Williams, 2005). Differences in

soil moisture resulting from these controls are subdued in lower portions of the watershed where there is not a sustained snowpack and in the upper watershed during periods of peak snowmelt when soil water inputs exceed available soil water storage capacities (Smith *et al.*, 2011). During spring snowmelt, when field capacities are exceeded, infiltrated water feeds streamflow via lateral soil and bedrock flow (Abdelmasih, 2006; McNamara *et al.*, 2005). The bedrock in the watershed is highly shattered with larger scale fractures throughout the watershed (Gates *et al.*, 1994). Groundwater contributions to streamflow are evidenced by numerous seeps and springs that feed Dry Creek and some of its tributaries observed by Aishlin (2006). During the winter months, geochemical evidence suggests that there are no inputs to streamflow from regional groundwater sources (Yenko, 2003). Throughout the entire watershed, as much as 11% (on average) of precipitation inputs go to groundwater recharge, while in some lower order sub-watersheds at higher elevations, up to 22% of precipitation inputs go to groundwater recharge (Aishlin, 2006).

1.6 Hypothesis Statement

Numerous studies conducted in the DCEW have identified differences in characteristics of north versus south facing hill slopes. North facing slopes are consistently steeper than south facing slopes and exhibit roughly planar hill slopes while their south facing counterparts are more dissected. Soils on north facing slopes are much deeper and finer than those on south facing slopes. Vegetation patterns also vary with slope aspect, with more voluminous and diverse vegetation occurring on north facing slopes. Within the framework of these observations, this thesis assesses whether

windblown sediment (dust) plays any role in soil development that may help to explain the differences observed on slopes of north and south aspects in the watershed and to address two key research questions:

- Is dust an important component of the soils of DCEW?
- If dust is important to these soils, how is it spatially distributed in the watershed?

The hypothesis is that the soils of the Dry Creek Watershed are strongly influenced by dust deposition. If this hypothesis is correct, the following trends should be observed:

- The chemical composition of the soils should indicate a mixture of compositional end-members loess and granodiorite.
- The silt fraction of the soils should comprise a greater percentage of the grain size distribution than if the soils were derived solely from bedrock because eolian dust is predominately silt-sized.
- The fine fraction of soils should exhibit compositions that closely resemble loess compositions.
- The loess chemical signature should have little variation as a function of elevation.
- The loess chemical signature should be stronger at shallower depths in the soil profiles because the flux of dust would enter the soil at the top of the soil profile.

- Loess chemical signature should be stronger in soils on north facing slopes than in those on south facing slopes because thicker, finer soils have been observed on north facing slopes,

2 METHODS

2.1 Site Selection

Eight soil pit sampling sites (LN, LS, MLN, MLS, MHN, MHS, HN, and HS) were selected within the study area (Figure 1) and were within 2 meters of sampling pits utilized in a previous study by Smith *et al.* (2011). These eight sites were originally selected and named by Smith (2010), and consist of four elevation-paired sites on opposing slope aspects. The rationale for selection of the sites were to 1) capture the elevation gradient within the study area, 2) evaluate differences in soils as a function of slope aspect, 3) capture the variable vegetation regimes associated with slope aspect and elevation differences, and 4) facilitate comparison to data from Smith (2010). The eight soil pits are located approximately at mid-slope locations in an attempt to characterize the representative geomorphic processes of each hill slope.

A total of six loess samples were collected from areas of the WSRP to the south and southwest of the study area from known loess deposits (see Figure 1). Utilization of loess as an end-member in the mixing model is justified by the assumption that windblown sediment that was delivered to the study area either shares the common source(s) with the WSRP loess deposits, is derived from the WSRP loess deposits, or is a combination of the two.

Identification of bedrock sampling sites was more challenging than for the soils and the loess because many of the soil pits utilized in this study exhibit a prohibitively deep zone of highly weathered saprolite. The approach was to identify bedrock samples that had undergone minimal weathering as the granodiorite end-member, so only ‘fresh’ clasts of bedrock that were found at the soil-bedrock interfaces were classified as bedrock. In four of the eight soil pits, ‘fresh’ bedrock was not found at the soil-saprolite interface, so three additional bedrock samples (RR-C, RR-G, and 8S-G) were identified and sampled from outcrops adjacent to the DCEW (see Figure 1).

2.2 Sample Collection

2.2.1 Collection of Soil Samples

Soil pits were excavated to the soil-bedrock/saprolite interface and cleaned of any material that had fallen from above during excavation. Soil sample intervals were determined through field interpretation of soil horizons, although all pits exhibit weak soil development. Often, separate horizons were not clearly evident, and in those cases soils were sampled from 10 cm depth increments with 5-10 cm left un-sampled between the sampled layers to avoid overlap. In all cases, care was taken to avoid sampling from areas showing obvious evidence of bio-turbation (for example, areas containing obvious lenses of material different than that of the overall soil matrix were not sampled).

2.2.2 Collection of Loess Samples

2.2.2.1 Loess Soils

Loess samples were collected in the same manner as described for DCEW soil samples in Section 2.2.1. All loess samples were extracted from modern weakly developed B-horizons or buried B-horizons.

2.2.2.2 Dust in the Snowpack

A snowpack profile from the upper DCEW was evaluated in an attempt to further constrain the composition of airborne material that is being deposited in the Boise Front. Samples were collected at 5 cm increments from a depth of 10 cm to 103 cm, melted and filtered through 40 μm nitrocellulose filters.

2.2.2.3 Airborne Dust

A preliminary dust sampling program was initiated at the Treeline Watershed (see Figure 1). Three prototype dust traps were distributed throughout the small, first-order watershed to evaluate the effectiveness of the design. The traps were based on the design described in Reheis and Kihl (1995), but slightly modified to eliminate any metal parts. The traps collected, on average, less than 14 mg of material, which was mostly organics and sand-sized lithic fragments from nearby hill slopes. The obvious contamination by local grains and the lack of adequate sample mass precluded any analysis of the samples.

2.2.3 Collection of Bedrock Samples

The dominant parent material for the soils within the study area is biotite granodiorite of the Atlanta lobe of the Idaho batholith. Clasts of minimally weathered

bedrock were sampled from the soil-bedrock interfaces of the soil sampling pits, where possible. In pits MLN, MHN, HN, and HS, bedrock clasts were suspended in more extensively weathered saprolitic matrices. In those cases, the saprolites were also sampled and characterized as soils. Bedrock samples were only taken at a location if the rock was relatively fresh and not ably broken by hand in the field. Three additional granodiorite samples were collected from outcrops located adjacent to the study area (see Figure 1).

2.2.4 Collection of Basalt Samples

The DCEW is proximal to several Miocene and younger basalt flows. To constrain the potential influence of basalt on soil chemistry in DCEW, three basalt ‘float’ samples were taken from hillsides below two basalt-capped outcrops to the west of the DCEW. Three additional samples of basalt were taken from Castlerock and Gowen Terrace areas to the southeast of DCEW.

2.3 Sample Preparation

All samples were prepared for elemental analysis by Inductively-Coupled Plasma Mass Spectrometry. The ensuing sections describe the methodology for preparation of soil samples, dust filtered from snowmelt, and airborne dust collected in a series of dust traps.

2.3.1 Whole Rock and Soil Fusions

All bedrock, soil, and loess soil samples were oven-dried for a minimum of 4 hours at 105°C. To minimize rehydration from atmospheric moisture, the dried samples

were quickly placed in airtight containers and frozen for storage. Immediately prior to sample processing, each sample was again dried for a minimum of 30 minutes at 105°C, and allowed to cool until comfortable to the touch.

All samples were homogenized and split using a variation of the cone-and-quarter method (Raab *et al.*, 1990). To homogenize, the full sample mass of each sample was poured onto a square sheet of clean paper, and successively ‘turned over’ into a cone on a second sheet of clean paper five times. Next, the cone was evenly split along the central axis of the cone parallel to the preferential pouring direction using a clean, dry knife. One of the original splits was placed in an airtight storage container and frozen for long-term storage, while the second of the splits was re-homogenized using the steps described above. This process was repeated until a desired sample mass of 50-60 g was achieved. The remaining sample from which the 50-60 g was sub-sampled was re-combined and placed in an airtight storage container and frozen for long-term storage. All procedural and replicate samples were subsequently sub-sampled from one of the original splits.

Selection of the cone method was based on several factors. It is a long-standing and well recognized method for sample homogenization and splitting (Schumacher *et al.*, 1990) and it is well suited to bulk sample masses exceeding 50 g (Müller, 1967). The method allows for concurrent homogenization and splitting of the bulk sample rather than a stepwise approach. While there is some concern regarding the loss of fines associated with the cone method, Schumacher *et al.* (1990) report that similar methods such as open and closed riffle splitter methods have comparable losses of fine material, within 10% of the cone method.

Some samples containing large rocks required one or more pre-crushing steps prior to powdering. When necessary, samples were wrapped in multiple layers of plastic and broken into smaller chunks using a sledgehammer. This step was executed carefully to minimize direct contact between the head of the sledgehammer and the sample. The samples were then crushed to approximately 1 cm in diameter using a large jaw crusher, then to approximately 0.25 cm with a small jaw crusher.

Following the requisite pre-crushing step(s), a modified lithium-tetraborate fusion method similar to that described by Jarvis *et al.* (1992) was used to achieve total dissolution of rock and soil samples, many of which contain hard-to-dissolve refractory minerals such as zircon. Samples were first ground to a fine powder in a SPEX CertiPrep Shatterbox using an alumina ceramic container that was cleaned and pre-contaminated before and after processing each sample. Approximately 300(\pm 2) mg of ground sample powder was mixed with 600(\pm 2) mg of Spectromelt lithium-tetraborate flux and homogenized using a vortex mixer. Samples were then transferred to clean carbon crucibles and placed in a muffle furnace at 900°C for 25 minutes to ensure complete melting. The resulting glass bead was cleaned of carbon residue from the crucible using ethyl alcohol, placed in a 500 ml HDPE bottle and brought to a final mass of 500(\pm 2) g using 2% HNO₃, 10 drops of concentrated HF, and 20 drops of concentrated H₂O₂ and placed on a platform shaker until full dissolution was achieved. The final sample dilution is approximate 1:1667, which is further diluted 2 times online during analysis. Solutions were analyzed for major, minor, and trace elements using a Thermo Scientific X Series2 Inductively-Coupled Plasma Mass Spectrometer (ICP-MS).

2.3.2 Acid Digestions

Filtered snow samples could not be dissolved using the Lithium-tetraborate fusion method due to concerns regarding sample loss by attempting to separate the sediment from the cellulose filters. Instead, Parr bomb acid digestions were performed for these samples and their associated filters. The procedure is detailed in the Appendix.

2.4 Estimating Loess Fractions in Soils Using a Two-Component Mixing Model

2.4.1 Two-Component End-Member Mixing Model

The research questions driving this study are 1) Is dust an important component in the soils of DCEW? and 2) If dust is important to these soils, how is it spatially distributed in the watershed? To address these questions, trends have been predicted that should reflect that dust is an important component in the soils distributed through DCEW. To help test some of these predicted trends, the approach is to utilize a simple tool to enable estimation of dust added to the soil; a simple two-component mixing model in which the granodiorite bedrock of the Boise Front and the loess deposits in the WSRP are compositional mixing end-members of the DCEW soils. The model is expressed as the following equation:

$$[L_i]x + [G_i]y = [S_i] \quad (\text{Equation 1})$$

Where: $[L_i]$ = concentration of element(s) i in the loess

$[G_i]$ = concentration of element(s) i in the granodiorite

$[S_i]$ = concentration of element(s) i in the soil

x = fraction of loess end-member in the soils

$y = (1 - x)$ = fraction of granodiorite end-member in the soils

L_i , G_i , and S_i have all been determined analytically and $(1 - x)$ can substitute for y so a value for the loess fraction x can be calculated for each of the soil samples as follows:

$$x = \frac{[S_i] - [G_i]}{[L_i] - [G_i]} \quad (\text{Equation 2})$$

Because loess is utilized as the end-member representing dust in this mixing model, the term ‘chemical loess fraction’ is used to describe the quantity x throughout this thesis.

2.4.2 Criteria for Mixing Model Inputs

The next step in the implementation of the mixing model was to identify what element or elements were the most suitable for input into the model. There were two criteria used for choosing the three elements used in the model (V, Co, and Cr). First, the elements must exhibit markedly different concentrations in the two end-members. Second, the elements must exhibit concentrations in the fine fraction of soils that are closer to the concentrations in the loess end-member than are the concentrations in its respective bulk soil. Figure 2 shows a plot of all elements analyzed with data points for the average bedrock concentrations, average loess concentrations, bulk soil concentrations, and fine fraction concentrations for one selected soil (MLN_0-10). V, Co, and Cr are highlighted in the plots to illustrate that they are the elements that best met the

two selection criteria. Chemical loess fractions for all soils were calculated (via Equation 2) using each of the three elements, then the three loess fraction values were averaged to represent the chemical loess fraction of the soil samples.

2.4.3 Mixing Model Assumptions

Utilization of the mixing model described in Section 2.4.1 requires that simplifying assumptions be made. Most importantly, it is assumed that the sampled loess and bedrock are representative mixing end-members for DCEW soils. This may be somewhat problematic for the loess end-member. Differentiation of grain size (and possibly chemical composition) between the dust that comprises the loess deposits in the WSRP and the dust incorporated into the DCEW soils may have occurred during deposition as a function of elevation and/or distance from source. Additionally, dust re-entrained from the WSRP and deposited in the DCEW may be further differentiated with respect to grain size and chemical composition. Despite these possibilities, it is reasonable to assume that dust added to the DCEW soils is chemically similar to the loess deposits in the WSRP. The composition of the bedrock end-member is better constrained but still requires some qualification. Bedrock clasts sampled from the bottom of soil pits were noticeably less weathered than the saprolitic matrices in which they were suspended, and remaining bedrock samples were extracted from bare outcrops that were obviously resistant to weathering. Hydrothermal alteration of the bedrock is widespread in the area and it is possible that the 'fresh' rock selected for sampling is preferentially resistant to weathering due to spatial variations in hydrothermal activity, potentially ascribing chemical compositions to the bedrock end-member that may not be

representative of all bedrock in the DCEW. However, since the alternative to sampling the freshest rock possible was to sample saprolite that is distinctly more weathered, the composition of the bedrock end-member is best represented by the least weathered samples.

The other major assumption in the mixing model is that the end-members are conservative. In other words, closed system conditions are assumed in which the chemical compositions of the end-members are not altered by chemical loss and redistribution through weathering, leaching, and erosion. This is not a realistic assumption and likely leads to some degree of overestimation of chemical loss fractions due to *in situ* enrichment of V, Cr, and Co (bedrock weathering is discussed in greater detail in Section 4.2). It is expected that inaccuracies resulting from this assumption are minimal and that the mixing model yields reasonable estimations of chemical loss fractions in Dry Creek soils.

2.5 Determination of Sample Variability

Sample variability was calculated as the quadrature sum of independent procedural variability and machine error. Procedural variability is reported as the relative percent difference of one standard deviation from the average of procedural triplicates for each sample class (bedrock, soil, and loess). Similarly, machine error is reported as the relative percent difference of one standard deviation from the average of four analyses of the same reference standard solution. Variabilities were determined for each element in all of the sample classes and are reflected as error bars on the plotted results of the data.

3 RESULTS

3.1 Loess Composition

3.1.1 Major Elements

The analytical results of major element composition of WSRP loess are presented in Table 1. Select major element oxides for the WSRP loess are plotted against Al_2O_3 (wt %) in Figure 3. For comparison, data is included in Figure 3 for loess sampled from Argentina, Europe, and Spitsbergen, Norway (Gallet *et al.*, 1998) and the Washington Palouse (Sweeney *et al.*, 2007). In both plots, the major element compositional range generally falls within the range occupied by the globally distributed loess sampled by Gallet *et al.* (1998). Overall, comparison of the data for all four major oxide pairings indicate that the WSRP loess generally falls within the loess compositional range reported in loess literature.

3.1.2 Trace Elements

The analytical results of trace element composition of WSRP loess are presented in Table 2. Relatively immobile trace elements (V, Cr, and Co) for the WSRP loess are plotted against Ti in Figure 4. For comparison, data is included in Figure 4 for loess sampled from Argentina, Europe, and Spitsbergen, Norway (Gallet *et al.*, 1998) and the Washington Palouse (Sweeney *et al.*, 2007). As with the major element comparison, the WSRP loess trace element compositional field generally falls within the range of globally

distributed loess although it should be noted that trace element concentrations in the global sample population vary by as much as an order of magnitude (for example Co concentrations vary from 3-32 ppm). No Co data was available for comparison for the Palouse loess.

3.1.3 Rare Earth Elements

The analytical results for Rare Earth Element (REE) composition of WSRP loess are presented in Table 3. Taylor *et al.* (1983) concluded that loess deposits are representative of the average composition of the continental crust. This claim is supported by the findings of Gallet *et al.* (1998), who reported remarkably similar REE pattern shapes in globally distributed loess samples and the average continental crust, irrespective of variable REE abundances. REE data for the WSRP Loess is presented in Figure 5 along with average REE values for the upper continental crust (Gallet *et al.*, 1998). All data is normalized to CI chondrite values from McDonough and Sun (1995). The WSRP loess samples exhibit nearly identical shapes of REE patterns as the upper continental crust, highlighted by light REE enrichment, a strong negative Eu anomaly and a broad flattening out of the heavy REEs. It is notable that all of the WSRP loess samples are enriched in overall REEs with respect to the average upper continental crust; however there is considerable variation on overall REE abundances in world-wide loess (Gallet *et al.*, 1998).

3.1.4 Dust in the Snowpack

A snowpack profile was evaluated in an attempt to further constrain the composition of airborne material that is being deposited in the Boise Front Range. Of the

19 samples from the profile, 3 contained sufficient material for analysis. Selected trace element data for the three profile depths are plotted against Cr in Figure 6. For comparison, dust collected from Colorado that is typical of that region (Reheis *et al.*, 2008) is also shown on the plots. DCEW snow-dust exhibits a wider range of Cr and Co concentrations than the Colorado dust, but less of a spread in Ni concentrations. There is marginal overlap of trace element compositional fields for both of the pairings presented, but the paucity of the DCEW snow-dust data precluded any further discussion of filtered snow dust.

3.2 Bedrock Composition

The bedrock of the Boise Front Range (and DCEW) area is medium to coarse-grained biotite granodiorite that is gray in color and mineralogically dominated by quartz and plagioclase feldspars, with 2-8 percent biotite (Johnson *et al.*, 1988). The bulk chemical compositions of the bedrock sampled in this study are presented in Tables 1-3. Selected major element oxides are plotted against Al_2O_3 in Figure 7, along with spatially distributed samples from the Atlanta Lobe of the Idaho batholith from Gaschnig *et al.* (2011) for comparison. Gaschnig *et al.* (2011) classifies the samples shown here as biotite granodiorite from the Atlanta peraluminous suite. DCEW granodiorite plots in the same major element compositional fields as the more widely distributed granodiorite data, indicating that the DCEW granodiorite is representative of other biotite granodiorite found in the Atlanta lobe of the Idaho batholith.

3.3 Soil Composition

3.3.1 Comparison of Soils to End-Members

The following sections compare the major, trace, and average REE compositions of the DCEW soils to the granodiorite bedrock and loess of the WSRP.

3.3.1.1 Major Elements

Major element oxides for DCEW bedrock, DCEW soils, and WSRP loess are presented in Table 1. Figure 8 shows plots of FeO and MgO against Al₂O₃ for the bedrock, soils, and loess. Iron and magnesium behavior is somewhat similar; however, iron is more enriched in the soils than magnesium relative to the bedrock. Both plots show a clear separation of loess and bedrock in compositional space and significant overlap of bedrock and soil compositions. The FeO-Al₂O₃ plot shows greater deviation between the bedrock and soils than the MgO-Al₂O₃ plot, and the soils appear to approximately occupy the compositional space between the bedrock and the loess. Overall, major element compositional fields show weak differentiation between the bedrock and soils and distinct separation of the loess from the two other fields.

3.1.1.2 Trace Elements

Selected trace elements (V, Co, and Cr) are plotted against Ti in Figure 9. Positive correlations are evident between all trace element and Ti concentrations with distinct zoning between bedrock and loess in compositional space. Bedrock compositions exhibit the lowest overall concentrations (1369-2357 ppm for Ti and 0.5-6, 1-2, and 1-2 ppm for V, Co, and Cr, respectively) while loess exhibits the highest overall concentrations

(3472-4622 ppm for Ti and 35-64, 8-16, and 31-44 ppm for V, Co, and Cr, respectively). The DCEW soils generally fall between the compositional fields of the bedrock and the loess, ranging from 1667-3499 ppm for Ti and 5-37, 1-8, and 1-22 ppm for V, Co, and Cr, respectively. V/Ti data (Figure 9a) shows slight encroachment of soil into both bedrock and loess fields. Two mid-depth soils from the LN site plot at or near the boundary of the loess field (LN_23-47 and LN_47-71) while two of the deepest soils in their respective profiles (LS_21-31 and MHS_80-90) plot near the bedrock field boundary. On the Co/Ti plot (Figure 9b), LN_23-47 and LN_47-71 again show overlap with the loess space while LS_21-31 and MHS_80-90 again show overlap with bedrock space. Another of the deepest soils in its respective profile (LN_94-117) encroaches on the bedrock in Co/Ti compositional space. Cr/Ti compositional space shows the most pronounced separation of the three fields (Figure 9c) with only one soil residing in the bedrock field (LS_21-31, the deepest soil at the LS site).

The same soil data plotted in Figure 9 are also shown in Figure 10, for V-Ti, Co-Ti, and Cr-Ti, respectively. To compare differences in soil trace element composition with respect to slope aspect and relative soil depth, the soils are broken down into four classes: north facing upper profile, north facing lower profile, south facing upper profile, and south facing lower profile. It is interesting to note that in all three of these plots, the soil class that exhibits the highest concentrations (i.e., plots closest to the loess field) is the 'north facing upper profile' class, while the 'south facing lower profile' class appears to most closely resemble the bedrock. Upper and lower soil profiles within each slope aspect bin show moderate overlap with the highest concentrations occurring in the upper

profile soils and the lowest concentrations in the lower profile soils, particularly with respect to V and Cr. Accordingly, when comparing north and south facing soils without regard to soil depth, V-Ti and Cr-Ti are generally elevated in the north facing soils while Co-Ti shows similar, but much less distinct behavior.

3.1.1.3 Rare Earth Elements

Average REE patterns for the bedrock, soils, basalt, and loess collected in this study are presented in Figure 11. This data is also presented in Table 3. All data is normalized to CI chondrite values from McDonough and Sun (1995). Average loess and average soil light REE data are nearly identical and exhibit enrichment with respect to average light REE data for the bedrock. The loess and soils exhibit more pronounced negative Eu anomalies than the average bedrock, but heavy REE data shows pronounced enrichment in the loess with respect to both the soils and bedrock. With the exception of La/Chondrite, the average REE distributions of the soils fall between the average REE distributions of the loess and bedrock.

3.3.2 Isolated Grain-Size Fractions

The fine sand and silt + clay fractions of the three soil depths sampled from the HS soil were analyzed for elemental composition. Figure 12 shows ratios of V/Ti, Co/Ti, and Cr/Ti for each grain-size isolate of the shallowest HS soil (0-10 cm depth), along with concentrations in the bedrock sampled from the HS pit, the bulk soil samples and average loess. The fine sand fraction consistently exhibit higher concentrations than the bulk soils, and concentrations in the silt + clay fraction are consistently higher than in the

fine sand fraction. Data from the other two depths at the HS site are similar to the 0-10 cm depth, and are not shown in the figure.

3.4 Local Basalt Composition

Select major element oxides are plotted against MgO in Figure 13. The basalt samples collected in this study are proximal to the Boise foothills and DCEW and are identified individually in each plot. The GT (Gowen Terrace A and B) basalts are Quaternary valley filling flows capping the Gowen Terrace of the Boise River (Othberg and Burnham, 1990) while the CR (Castlerock) and FH Foothills (High, Middle and Low) basalts are part of the Miocene aged Boise Assemblage (Wood and Clemens, 2002). For comparison, type M1 (late Miocene) basalts, and M2 and M3 (late Pliocene to early Pleistocene) basalts from near Weiser, Idaho (White *et al.*, 2002) are included in the figure. All of the sampled basalts generally occupy the same major element compositional space as the Weiser basalts. The GT-B sample plots either within or very near the youngest M3 Weiser basalts, while GT-A sample plots near the M2 Weiser basalts. The CR basalt generally plots outside of all Weiser basalt fields in Figure 13, but consistently plots between the M2 and M3 Weiser basalts. The three FH basalts correspond with the Weiser M1 basalt. Although highly variable, the major elemental compositions of the basalts sampled in this study are similar to those from White *et al.* (2002) and appear to be representative of local basalt compositions.

3.5 Chemical Loess Fraction Estimates

Chemical loess fractions in all DCEW soils were estimated using the method described in Section 2.4 and are reported in Table 4. Estimates range from 0.02 at the LS site (21-31 cm depth) to 0.63 at the LN site (47-71 cm depth), with an average of 0.28 for all soils. Chemical loess fractions are consistently higher in soils on north facing slopes (minimum of 0.12, maximum of 0.63, and average of 0.38) than in soil on south facing slopes (minimum of 0.02, maximum of 0.29, and average of 0.16).

4 DISCUSSION

4.1 Evaluation of Predicted Trends

The predicted trends outlined in Section 1.6 are most effectively addressed by examining the behavior of the relatively immobile trace elements (V, Co, and Cr). Since the greatest compositional differences between the bedrock and the loess exist in V-Ti, Co-Ti, and Cr-Ti compositional spaces, these ratios are best suited to assess how the composition of the DCEW soils relate to the end-member populations. The following sections utilize the plotted elemental data presented in the Results section and/or chemical loess fraction estimates (Table 4) to evaluate the predicted trends.

4.1.1 Soils as a Product of Mixing

If the soils are a mixture of the two hypothesized end-members, they should occupy the compositional space between the compositional spaces of the end-members. Figure 9 shows, with minor exception, that the DCEW soils plot directly between the bedrock and the loess end-members in compositional space. One would expect a population to follow a continuum in any mixing scenario, and the few exceptions evident in the figure can be explained qualitatively. The soils that plot in bedrock space are the deepest soils in their respective profiles, so it is not surprising that their composition is so similar to that of the bedrock. The overlap of soils with the loess field may result from two compounding factors. First, the soils that plot in that space are mid-depth soils from

the LN soil pit, which contained an abnormally high amount of fine-grained material when compared to the other sites. Second, the loess sample exhibiting the lowest trace element concentrations (GT_20-30) was taken from a section of the soil profile exhibiting less pedon development than the other two samples from that profile, perhaps differentiating it from the others in terms of trace metal enrichment resulting from translocation of clays during soil development. Regardless of the few exceptions, comparison of the trace element compositions of the soils and end-members suggests that the DCEW soils are a mixture of loess and granodiorite.

4.1.2 Grain-Size Distribution

Does silt comprise a greater percentage of the grain size-distribution than if the soils were derived solely from granodiorite? This question requires the assessment of what should be expected in terms of grain-size distribution without loess influence. It is traditionally thought that in situ weathering of crystalline rocks results in a bimodal grain-size distribution in soils, with one peak centered in the clay-sized fraction and another centered in the sand fraction (Walker *et al.*, 1988; Bremer, 1980). From a chemical weathering standpoint, it is reasonable to expect the dissolution of larger primary mineral crystals to be accompanied by the formation of secondary clays and oxides in the clay-sized fraction (Brady and Weil, 1999). Thus, it stands to reason that the presence of a significant fraction of silt-sized particles would require silt influx to the soils from an outside source. Figure 14 shows the grain-size distribution curves of four shallow DCEW soils, with ranges for granodioritic saprolite and loess for comparison. The silt content for the LN, MHN, MHS, and LS soils are approximately 33, 20, 13, and

8 percent, respectively, whereas a maximum of 8 percent silt content is estimated in the saprolites. All four of the soils exhibit silt fractions equal to or greater than the silt content in saprolites. The shape of the distribution curves for the soils with the highest silt content (LN and MHN) mimic the shape of the loess range in the finer fractions, showing modal peaks at the sand/silt boundary, and not in the clay fraction, while the LS soil shows a minor modal peak in the fine silt and clay fractions. Comparison of the grain-size distribution curves indicate that the LN, LS, and MHN soils generally have finer textures than the saprolites, and that the LN and MHN soils contain distinctly higher fractions of fine sand and silt than the saprolites. Figure 15 shows the percent increase of silt content in all pit-averaged soils (data from Smith *et al.*, 2011), relative to the average silt content in the saprolites. Increases range from less than 1 percent in the MHS soils to nearly 240% in the LN soils. On average, the south facing soils increase 24 percent and north facing soils increase 139 percent. This comparison of grain-size data supports the hypothesis that a significant volume of windblown dust has accumulated in portions of the DCEW.

4.1.3 Soil Fine Fractions

Do the fine fractions of DCEW soils exhibit compositions that more closely resemble loess compositions than do the associated bulk soils? If predominately silt-sized dust particles have been mixed into the soils, the fine fraction of the soils should reflect compositions more similar to the loess end-member. The data shown in Figure 2 illustrates that the concentrations of V, Co, and Cr are high in loess, low in the bedrock, and are enriched in the finer fractions of the MLN (0-10 cm depth) soil relative to the

bulk soil composition. This trend is also evident in the HS site soil profile. The fine fraction (fine sand and silt + clay) of the three soils sampled from the HS site were analyzed for elemental composition. Figure 12 shows data from the shallowest soil at the HS site (0-10 cm depth) and is representative of data in the full HS profile, illustrating Cr/Ti, V/Ti, and Co/Ti ratios of the fine fraction isolates along with those in the bedrock sampled from the soil/bedrock interface in the HS soil pit, the bulk soil samples, and the average loess. These ratios systematically increase from bedrock through bulk soil, fine fraction isolates and loess, indicating that the compositions of the fine fractions of soils in the HS soil profile more closely resemble loess in composition than do their associated bulk soils.

4.1.4 Elevation

Based on observations of similar soil depths (excluding slope aspect differences) across the elevation gradient of the DCEW, a clear trend was not expected when considering loess chemical signal strength across the elevation gradient of the DCEW. It was suspected that the signal might be slightly stronger at lower elevations because the energy required to carry material to higher elevations is greater, however no identifiable trend was observed. The minimum, maximum, average, and standard deviations of estimated loess fractions for the soils at each N-S elevation pairing are reported in Table 5. One notable difference between the four elevation groups is that the lowest loess fraction estimate at the high elevation sites was approximately 0.20, which is significantly higher than for the other elevations. While one might speculate that this could result from some mechanistic difference related to elevation (temperature or

precipitation), it should be noted that the mid-low sites also had a larger minimum (approximately 0.10 chemical loess fraction), while the minimums for the low and mid-high sites were almost zero. Beyond that, any influence that elevation may have had on loess chemical signal strength appears to be small enough to be overshadowed by other influences.

4.1.5 Soil Depth

If there were dust being added to the soils through eolian transport, the influx would enter the soil profile from the top. Accordingly, evidence of a gradient in dust content was expected, with the highest content in the upper portions of soil profiles and the lowest content in deeper portions of soil profiles. Figure 16 shows the chemical loess fractions estimated for all soils plotted against the depth from which each of the soils was sampled. When considering north and south soils together, no visual trend is evident with depth, but the average chemical loess fraction in the upper half of soils is greater than in the lower half (0.31 and 0.23, respectively). When considering the north and south soils separately, the trend with depth becomes more evident within each population. The average loess fraction for upper half north facing soils is 0.42 compared to 0.32 for lower half north facing soils. The difference between upper and lower half south facing soils is similar (0.20 and 0.12, respectively). The data shown in Figure 10 supports this interpretation, showing that soils in the upper half of soil profiles generally plot closer to the loess compositional field than those in the lower half, within each aspect class. These data suggest the loess chemical signature is, on average, stronger in shallower soils than deeper soils.

4.1.6 Slope Aspect

Field observations by this author and others (Geroy *et al.*, 2011; Smith, 2010; Tesfa *et al.*, 2009) in DCEW indicate that soils on north facing slopes are markedly deeper than those on south facing slopes. While these differences are influenced by slope aspect related differences in insolation and vegetation type, these observations drive the question of whether loess could preferentially accumulate on north facing slopes. If it is assumed that loess supplied to DCEW is sourced from the WSRP to the south and southwest, then it is reasonable to suspect that dust-loaded winds that enter the DCEW blow from the south and southwest. Although prevailing winds in Boise seasonally shift from ENE to WNW, 17 percent of peak monthly wind gusts exceeding 15 m/s were S or SW (NOAA, n.d.). Studies of grain deposition mechanics suggest that topographic barriers create turbulences leading to lower wind energy fields on leeward slopes (Goossens and Buck, 2011; Van Boxel *et al.*, 1990). Thus, it is reasonable to expect that S and SW dust-laden winds may preferentially deposit more loess on north facing slopes than on south facing slopes, and the loess chemical signal should reflect that.

Additionally, the presence of more extensive and denser vegetation on north facing slopes may further help to reduce wind-speeds, act as traps to promote dust deposition, and subsequently protect the dust from re-entrainment. Figure 17 shows that loess fraction estimates in north facing soils are more than twice as high as those in south facing soils (0.38 and 0.16, respectively). The data presented in Figure 10 also supports this interpretation, showing that in compositional space, north facing soils generally plot closer to the loess field than do south facing soils, and the relationship holds true within

the soil depth classes. Thus, the evidence clearly suggests the chemical signature of the loess end-member is stronger in soils on north facing slopes than in soils on south facing slopes.

4.2 Other Possible Explanations for DCEW Soil Characteristics

4.2.1 Weathering of Bedrock

One alternative explanation to dust addition for the Dry Creek soils is that *in situ* weathering of granodiorite bedrock produces the observed soil chemistry and grain-size distributions. The following discussion compares the data from Dry Creek to chemical and grain-size data from other studies to evaluate the possibility that bedrock weathering alone could explain the observed soil characteristics in the DCEW.

Chemical trends in granitoid weathering have been studied in a variety of landscapes and climates. Nesbitt and Markovics (1997) studied weathering of granodiorite in southern Australia. The Australian granodiorite forms a highland plateau in an area receiving more than twice as much precipitation (1500 cm) as Dry Creek (700 cm) (Nesbitt and Markovics, 1997). These conditions promote more rapid bedrock weathering than conditions in Dry Creek due to more precipitation and subdued topography. Nesbitt and Markovics (1997) report maximum enrichment of V/Ti and Cr/Ti ratios in regolith of 17% and 146%, respectively and attribute much of the enrichment to residuals from previously eroded regolith. For comparison, the average enrichments of V/Ti and Cr/Ti in Dry Creek soils (with respect to average bedrock) are 245% and 517%, respectively. In a climate similar to the Nesbitt study, Tijani *et al.*

(2006) reports maximum enrichment (from granitic bedrock to soil) in V and Cr as 51% and 95%, respectively, while the average enrichments of V and Cr in the Dry Creek soils are approximately 350% and 1000%, respectively (see data in Table 2). On average, V, Cr, and Co increase by a factor of five from the granodiorite to the soils (see data in Table 2). If these trace elements were completely conserved in the soils system, these concentrations would require the loss of 80% of the regolith, and that magnitude of lost mass should be reflected in marked differentiation of major element chemistry between the bedrock and soils. As seen in Figure 8, ratios of the oxides of major mobile elements (FeO and MgO) versus immobile oxide (Al_2O_3) show little differentiation when comparing bedrock to soils. These conservative comparisons illustrate two points: it is very likely that weathering of *in situ* bedrock contributes to enrichment of V and Cr in Dry Creek and that process does not appear to be the dominant mechanism of trace metal enrichment in Dry Creek.

Over the last few decades, investigations have placed increased emphasis on the effectiveness of physical and chemical weathering on zonal weaknesses in quartz grains as it relates to *in situ* production of silt-sized particles in soils (Nahon and Trompette, 1982; Pye, 1987; Smith *et al.*, 2002; Wright *et al.*, 1998). Frost shattering, insolation cracking, salt weathering and crack fill by expanding clays may all contribute to *in situ* generation of silt-sized grains. Additionally, the hydrothermal alteration of the bedrock in the Boise Front may have further exploited zonal weaknesses in crystals. Field observations of high silt percentages in crystalline rock derived soils are typically found in more humid and warm equatorial regions where chemical weathering can progress

more rapidly than in semi-arid regions (Nahon and Trompette, 1982). Conversely, Kwon and Oh (2011) studied decomposed granite soils in China, reporting that less than 5% of soil grains are in the silt-sized and clay-sized fractions. Extensive weathering should produce clearly defined soil horizons with distinct zones of illuviated clays, but Dry Creek soils show very little development, with no distinct B-horizons. While physical weathering processes likely contribute to silt grain production in the DCEW soils, poor development of the DCEW soils, highlighted by very low clay content and indistinct zones of illuviation suggests weathering does not drive significant *in situ* production of silt-sized grains from the crystalline bedrock.

4.2.2 Basalt Influences

Because of the close proximity to several basalt flows and the presence of mafic dikes in the Boise Front, it was suspected that basalt may be an end-member in a two-component (basalt-granodiorite) or three-component (basalt-loess-granodiorite) mixing scenario. In terms of chemical composition, these materials are distinctly different. Granodiorite lies near the felsic end of the compositional spectrum, basalt at the mafic end, and loess is of intermediate composition. The dynamics of the partial melting process depletes the less mobile elements in felsic igneous rocks. The elements selected for use in the mixing model (V, Cr, and Co) are among those that are depleted in the granodiorite relative to loess and basalt. When comparing the bedrock, DCEW soils, loess, and basalt in V/Ti compositional space, the basalt field lies along the same trajectory as the other populations, and the high concentrations of V and Ti in basalt suggest that if basalt were an end-member, the trace element mass balance would require

only a small amount of basalt mixing with bedrock to achieve the observed soil trace element compositions. Figure 18 shows the data from Figure 9 along with data for the six basalt samples from near the study area. It should be noted that the Cr and Co data plot similarly, so only the V and Ti data is shown in Figure 18.

Despite the trace element data supporting basaltic influence on the DCEW soils, there is qualitative and quantitative evidence suggesting that basalt is not a mixing end-member. No visual evidence of basaltic clasts was noted during the field sampling campaign. The micro-crystalline structure of basalt precludes production of silt-sized grains from basalt weathering, leaving abnormally high silt content in DCEW soils unexplained by basalt influence. Weathering products of basalt are almost exclusively secondary clay minerals and hydroxides, suggesting that DCEW soils should have more in the clay-sized fraction content than is observed. Because basalt is enriched (relative to the bedrock) in many trace elements, it is difficult to chemically discount that basalt influences the soils. However, the behavior of U provides the basis for this argument. Figure 19 shows a plot of U versus Ti concentrations for the bedrock, soils, loess, and basalt. In U-Ti compositional space, it appears that the soils plot between the space occupied by the bedrock and loess fields, which is consistent with the trace elements plotted in Figure 9. Within the soils data field, concentrations of U and Ti appear to have an increasing trend toward the loess field, which is not supported by the low U concentrations in basalt. It should be noted that basaltic influences cannot be completely ruled out. The geology of the Boise Front Range and the WSRP suggests that there may be a basaltic component in loess, making it difficult to clearly discern between loess and

basalt as potential end-members. However, the body of evidence (U chemistry, grain-size distributions, and field observations) supports the hypothesis that loess is the mixing end-member to soils in the Dry Creek soils.

4.2.3 Other Influences

In addition to the potential for in situ bedrock weathering and basalt to influence DCEW soil properties, and how we interpret them, there are a number of other influences that may help to explain spatial variations in soil properties in the watershed. The following discussion addresses some of those possibilities.

Soils of the steep-sloped Idaho batholith are estimated to lose 1cm/1000yr, a rate substantial enough to inhibit even moderate soil horizon development (Clayton *et al.*, 1979). Batholith soils are typically shallow (1-3 m) and poorly developed (Clayton *et al.*, 1979). Soils in the DCEW are no exception, with no distinct differentiation of clay content in depth profiles (Smith, 2010). The physical loss of soil mass through erosion may concurrently confound and help the argument that loess is influencing the soils. On one hand, it is difficult to discern the chemical composition of the eroded material, and to account for that in the mixing model. Additionally, dust added to the soil enters at the top of the profile, and it is from the top of the profile that material is physically removed during erosion events. To counter those points, one could argue that if material were removed from the upper profile, there is no reason to suspect that physical removal of the upper soil would chemically differentiate the remaining material such that it would be more enriched in trace elements. In fact, it could be argued that the erosion of the upper

portion of the soil profile (most enriched in Co, V, and Cr) may preferentially subdue the loess chemical signature in the soils.

Soils develop through the influences of five soil forming factors: climate, organics, topography, lithology, and time (Jenny, 1941). Differences in the DCEW soils reflect spatial differences in micro-climate across the watershed. Interpretation of results presented herein is confounded by possible influences, and feedbacks of those influences that affect the physical and chemical nature of the soils. There is a substantial elevation difference from the lower portion of the watershed to the upper portion of the watershed, leading to differences in both temperature and precipitation. At lower elevations, temperatures are higher, and there is less precipitation with no season-long snowpack, while higher elevations receive an orographically induced increase in precipitation and colder temperatures, supporting a sustained winter snowpack. Thus, the timing and amount of precipitation input is vastly different in different portions of the watershed. Additionally, differences in insolation exist when comparing north and south facing slopes. Insolation is potentially twice as high on south facing slopes (Smith, 2010), which drives increased evaporation and snowmelt. It is reasonable to suspect that these collective differences in temperature and precipitation inputs across the watershed influence the rate of physical and chemical weathering differently at different locations.

Climatic influences also contribute to differences in vegetation. At lower elevations in DCEW, south slopes are dominated by grasses, while north slopes have a mixture of grasses, brush, and shrubbery. At mid elevations, the difference is more distinct, with the occurrence of Douglas fir and pine species on north slopes and

predominately grasses on south slopes. At upper elevations, conifers dominate both slopes. Differences in vegetation among these sites may influence soil depth and chemical characteristics in a number of ways. Soils dominated by conifers may be more resistant to mass movement because root structure provides increased support to the soils, and also may be more resistant to erosion from rain impact because of the protective canopy, but these soils would be subject to diffusive erosion by tree root throw over longer timescales. Differences in nutrient uptake and sequestration time between these climate-driven vegetation differences may also affect soil chemistry at different timescales. More voluminous and diverse vegetation may create a more favorable depositional environment for loess on the north facing slopes, and in turn, the resultant addition of fine-grained material and nutrients could further promote vegetation that promotes accumulation.

It is difficult to quantifiably differentiate between influences on soil development because they are intermingled with a complex series of feedbacks. Collectively, it is reasonable to suspect that these influences contribute, at least in part, to the chemical and physical properties of DCEW soils that have been attributed to loess addition.

4.3 Ecohydrological Implications of Loess Inputs to Dry Creek Soils

A natural extension of the research questions driving this study is to evaluate the impact of loess addition to DCEW soils. If the mixing model defined and discussed herein is a representative way to quantify the amount of loess in the soils, then it is possible to assess what the soil characteristics would be like without their addition.

Figure 20 shows a comparison of the pit-averaged chemical loess fractions and the pit-

averaged silt content in equivalent pits by Smith (2010). Although it is evident that the loess fraction model does not agree perfectly with the measured silt content and that it appears to over predict in some cases, there is reasonable correlation between the two data sets ($R^2 = 0.77$).

The approach to make this evaluation is conceptually simple. First, the field capacity of the soils is evaluated under their present classification and the estimated chemical loess fraction is removed from the silt fraction, then the resultant soil textures are reclassified and field capacities are re-evaluated. For example, if a soil contains 50% silt, 40% sand, and 10% clay, and the chemical loess fraction model estimates a loess contribution of 40%, then that 40% is removed and the remaining fractions (10% silt, 40% sand, and 10% clay) are normalized to the remaining 60% (of original) total. To allow comparison between current and predicted soil textures, empirically derived values of field capacity for soils in their current states are not used here. Instead, field capacities for both current and predicted soil textures are classified using a generalized soil texture/water content curve from Fetter (2001). A value for soil dry condition of 0.03 is assumed for all sandy soils in the predicted scenario. Bulk density is assumed equal for both scenarios. Note that if the loess fraction exceeds the silt fraction, only the silt fraction is removed. It is reasonable to suspect that significant additions of dust to soils may also increase the overall depth of the soils, and therefore the soil water storage capacity. However, the coarse nature of soils derived from crystalline rocks (Kwon and Oh, 2011) may provide adequate pore space to allow for incorporation of large volumes of fine-grained material without affecting overall soil depth. Accordingly, evaluation of

soil water storage capacities in this exercise ignores any potential increase in soil depth that may result from dust addition, instead focusing solely on textural changes.

Table 6 summarizes the results of this exercise. For all of the soil pits except LN, the soil changed from loamy sand or sandy loam (as classified by Smith, 2010) to sand (LN remained as sandy loam). The coarsening of the soils results in a reduction of soil water storage capacities of up to 9.2 cm (59%), with an average decline of 5.3 cm (48 %) for soils in the DCEW. This simplistic approach illustrates the potential importance of dust inputs to soils in the Boise Front. Smith *et al.* (2011) suggest that soil water storage capacities cannot fully accommodate spring snowmelt in the DCEW, and that water stored in the soil is quickly removed by evapotranspiration in the spring growing season, leaving spring rain as the primary control on soil moisture during the growing season. Without the influence of dust inputs to the soils, it is expected that reduced soil water storage capacities would make DCEW soils more sensitive to spring rain inputs and the soils would reach soil dry conditions earlier in the dry summer season.

Climate, soil characteristics, and vegetation are primary controls on soil moisture dynamics (Rodriguez-Iturbe *et al.*, 2001). Accordingly, spatial variations in soil water controlled by soil texture and porosity are often reflected in vegetation patterns. However, very few correlations between distinct soil characteristics and vegetation have been established (Hironaka *et al.*, 1991). A particular plant species can be the dominant species in coarse soils in dry climates, and also in fine soils in wet climates (Fernandez-Illescas *et al.*, 2001). This phenomenon, known as the ‘inverse texture effect’, occurs primarily because soil moisture loss in dry climates occurs more quickly through

evaporation from the upper profile than loss via vertical flow from the deeper profile (Noy-Meir, 1973). Because soil water availability at preferential depths can occur in soils with vastly different characteristics in different climates, it is problematic to make broad correlations between vegetation and soil characteristics. In contrast, relationships between soil properties and vegetation can be much stronger at watershed scales. In the DCEW, soils with finer textures are consistently wetter throughout the year (Smith, 2010; Geroy *et al.*, 2011). These differences in soil moisture are reflected in distinctly different vegetation regimes, particularly in the lower and middle elevations in the watershed. Theoretical removal of fine material in the DCEW soils (described in the previous paragraphs) results in sandy soils at nearly all sites, removing the spatial variation of soil properties across the watershed. This would remove soil properties as a primary control on differentiation of soil moisture states, leaving microclimate influences as the primary controls. Regardless of how soil moisture states (and vegetation) would be differentiated under those conditions, the overall water storage capacities in DCEW soils would be reduced, and the duration of the growing season shortened.

4.4 Suggestions for Future Work

This study provides geochemical evidence for the addition of loess to the DCEW soils. However, several lines of investigation would serve to strengthen the argument. Comprehensive mineralogical analysis coupled with elemental analysis of the mineral isolates of the loess, bedrock, and soils would help to clarify the evolution of trace element enrichment during soil mixing and weathering. Isotopic investigations would provide better end-member constraint, help to elucidate the provenance of the loess, and

provide a better constrained mixing model. Loess collection using dust traps distributed through DCEW would help to better constrain the airborne dust composition. Simulated weathering experiments of the granodiorite bedrock may help to constrain the ability of these rocks to produce silt-sized grains *in situ*, and help to identify preferential mineral phases for conservative elements.

CONCLUSIONS

The physical and compositional characteristics of spatially distributed soils, granodiorite bedrock, and loess were utilized to evaluate a series of predicted trends. The two end-members exhibit markedly different trace element compositions and, in compositional space, the soils fall between the end-member fields, suggesting that they are a mixture of the two end-members. The silt fraction of the soils in the DCEW are generally higher than literature indicates they should be from bedrock weathering alone, implying that silt must have been added from outside of the profile. The compositions of soil fine fractions in selected soils resemble loess compositions more closely than their associated bulk soils. No distinct trend in estimated loess fraction was identified as a function of elevation. Soils in the upper portions of soil profiles exhibit compositions closer to that of the loess end-member than do soils in the lower portions of profiles. There is a distinct relationship between slope aspect and the loess chemical signal in the DCEW soils, with estimates of chemical loess fraction on the north slopes (38%) more than doubling those on the south slopes (16%). Two component mixing model calculations suggest that soils in the DCEW contain an average of 28% dust. Collectively, these pieces of evidence indicate that the soils of the Dry Creek Experimental Watershed are strongly influenced by dust deposition. Without the addition of dust, currently limited soil water storage capacities may be reduced by an average of 5.3 cm, reducing summer soil water availability by an average of 48% in Dry Creek soils.

REFERENCES

- Abdelmasih, D.M.M. 2006. Influence of Saturated Wedge Hydrodynamics on Hillslope-Stream Connectivity, Department of Geosciences, Hydrologic Sciences, Boise, Idaho, Boise State University, Masters of Science.
- Aishlin, P.S. 2006. Groundwater Recharge Estimation Using Chloride Mass Balance Dry Creek Experimental Watershed, Department of Geosciences, Hydrologic Sciences, Boise, Idaho, Boise State University, Masters of Science.
- Austreng, A., Perrault, L. and M. Poulos. 2010. Investigating the Occurrence of Loess in the Soils of Dry Creek Experimental Watershed, Idaho. unpublished data.
- Brady, N.C. and R.R. Weil. 1999. *The Nature and Property of Soils*. Upper Saddle Hall, NJ: Prentice Hall.
- Bremer, H. 1980. Landform development in the humid tropics, German geomorphological research. *Zeitschrift für Geomorphologie*, Supplementband; 36:162–175.
- Chadwick, O.A., and J.O. Davis. 1990. Soil-forming intervals caused by eolian sediment pulses in the Lahontan basin, northwestern Nevada, *Geology*; 18:243–246, DOI:10.1130/0091-7613(1990)018<0243: SFICBE>2.3.CO;2.
- Clayton, J. L., Megahan, W.F. and D. Hampton. 1979. Soil and bedrock properties—weathering and alteration products and processes in the Idaho Batholith. Res. Pap. INT-237. Ogden, UT: U.S. Department of Agriculture, Forest Service, Intermountain Forest and Range Experiment Station. 35 pp.
- Clemens, D.M., and S.H. Wood. 1993. Radiometric dating, volcanic stratigraphy, and sedimentation in the Boise foothills, northeastern margin of the western Snake River Plain, Ada County, Idaho: *Isochron/West*; 59:3-10.
- Dahms, D.E. 1993. Mineralogical evidence for eolian contribution to soils of late Quaternary moraines, Wind River Mountains, Wyoming, USA, *Geoderma*; 59:175–196, DOI:10.1016/0016-7061(93)90068-V.
- Dahms, D.E. and C.L. Rawlins. 1996. A Two-Year Record of Aeolian Sedimentation in the Wind River Range, Wyoming, U.S.A., *Arctic and Alpine Research*; 28(2):210-216.
- Ferrier, K.L., Kirchner, J.W. and R.C. Finkel. 2011. Estimating millennial-scale rates of dust incorporation into eroding hill slope regolith using cosmogenic nuclides and

- immobile weathering tracers, *Journal of Geophysical Research*; 116, F03022, DOI:10.1029/2011JF001991.
- Fernandez-Illescas, C.P., Porporato, A., Laio, F. and I. Rodriguez-Iturbe. 2001. The ecohydrological role of soil texture in a water-limited ecosystem, *Water Resources Research*; 37(12):2863-2872.
- Fetter, C.W. 2001. Applied Hydrogeology, 4th ed., Prentice Hall, Inc., Upper Saddle River, New Jersey 07458.
- Gallegos, D., P. Johnson, S. Wood, and W. S. Snyder. 1987. Depositional facies patterns along the Boise front, *Northwest Geology*; 16:47–59.
- Gallet, S., Jahn, B., Lanoë, B.V.V., Dia, A. and E. Rossello. 1998. Loess geochemistry and its implications for particle origin and composition of the upper continental crust, *Earth and Planetary Science Letters*; 156:157-172.
- Gaschnig, R.M., Vervoort, J.D., Lewis, R.S. and B. Tikoff. 2011. Isotopic Evolution of the Idaho Batholith and Challis Intrusive Province, Northern US Cordillera, *Journal of Petrology*; 52(12):2397-2429.
- Gates, W.C.B., Parkinson, C.L. and K.L. Schroeder. 1994. Groundwater development in granitic terrain, Bogus Basin ski resort, Boise, Idaho. Hydrogeology, Waste Disposal, Science and Politics Proceedings 30th Symposium, Engineering Geology and Geochemical Engineering.
- Gillette, D.A., Adams, J., Endo, A., Smith, D. and R. Kihl. 1980. Threshold Velocity for Impact of Soil Particles into the Air by Desert Soils, *Journal of Geophysical Research*; 85(10):5621-5630.
- Geroy, I.J., Gribb, M.M., Marshall, H.P., Chandler, D.G., Benner, S.G. and J.P. McNamara. 2011. Aspect influences soil water retention and storage. *Hydrologic Processes*; 25:3836-3842, DOI:1002/hyp8281.
- Goldstein, H.L., Reynolds, R.L., Reheis, M.C., Yount, J.C. and J.C. Neff. 2008. Compositional trends in aeolian dust along a transect across the southwestern United States, *J. Geophys. Res.*; 113, F02S02, DOI:10.1029/2007JF000751.
- Goossens, D. and B. Buck. 2011. Gross Erosion, Net Erosion and Gross Deposition of Dust by Wind: field data from 17 surfaces, *Earth Surface Processes and Landforms*; 36:610-623.
- Hironaka, M., Fosberg, M.A. and K.E. Neiman. 1991. The relationship between soils and vegetation. Presented at the Symposium for Management and Productivity of Western-Montaine Forest Soils, Boise, ID, April 10-12, 1990.
- Jarvis, K.E., Gray, A.L. and R.S. Houk, 1992. Handbook of Inductively Coupled Plasma, Blackie, London. pp. 196-200.
- Jenny, H. 1941. Factors of Soil Formation, Dover: New York. 191 pp.
- Jickells, T.D., An, Z.S., Anderson, K.K., Baker, K.R., Bergametti, G., Brooks, N., Cao, J.J., Boyd, P.W., Duce, R.A., Hunter, K.A., Kawahata, H., Kubilay, N., LaRoche,

- J., Liss, P.S., Mahowald, N., Prospero, J.M., Ridgwell, A.J., Tegen, I. and R. Torres. 2005. Global Iron Connections between Desert Dust, Ocean Biogeochemistry, and Climate, *Science*; 308(5718):67-71.
- Johnson, K.M., Lewis, R.S., Bennett, E.H. and T.H. Kiilsgaard. 1988. Cretaceous and Tertiary intrusive rocks of south-central Idaho, in Link, P.K. and W.R. Hackett, (eds), Guidebook to the Geology of Central and Southern Idaho: *Idaho Geological Survey Bulletin*; 27:55-86.
- Kunkel, M.L., Flores, A.N., Smith, T.J., McNamara, J.P. and S.G. Benner. 2011. A Simplified Approach for Estimating Soil Carbon and Nitrogen Stocks in Semi-arid Complex Terrain, *Geoderma*; 165(1):1-11.
DOI:10.1016/j.geoderma.2011.06.011.
- Kwon, Y. and S. Oh. 2011. Physical and mechanical properties of decomposed granite soils sampled in Cheongju, Korea, *International Journal of the Physical Sciences*; 6(24):5777-5794, DOI:10.5897/IJPS11.1127.
- Laio, F., Porporato, A., Ridolfi, L. and I. Rodriguez-Iturbe. 2001. Plants in water-controlled ecosystems: active role in hydrologic processes and response to water stress II. Probabilistic soil moisture dynamics, *Advances in Water Resources*; 24:707-723.
- Lawrence, C.R., Neff, J.C. and G.L. Farmer. 2011. The accretion of aeolian dust in soils of the San Juan Mountains, Colorado, USA, *Journal of Geophysical Research*, 116, FE2013, DOI:10.1029/2010JF001899.
- Lewis, G.C., Fosberg, M.A., McDole, R.E. and J.C. Chugg. 1975. Distribution and Some Properties of Loess in Southcentral and Southeastern Idaho, *Soil Sci. Soc. Amer. Proc.*; 39:1165-1168.
- McDonough, W.F. and S.S. Sun. 1995 Composition of the Earth, *Chemical Geology*; 120:223-253.
- McNamara JP, Chandler D, Seyfried M and S. Achet. 2005. Soil moisture states, lateral flow, and streamflow generation in a semi-arid, snowmelt-driven, catchment. *Hydrological Processes*; 19:4023-4038, DOI: 10.1002/hyp.5869.
- Müller, G. 1967. Methods in Sedimentary Petrology. In: Van Engelhart, B.W. *et al.*, *Sedimentary Petrology*, Part 1. Hafner Publishing Co., New York. 283 pp.
- Muhs, D.R. 2007. Loess deposits, origins and properties. In: Elias, S.A. (ed), *Encyclopedia of Quaternary science*, Amsterdam: Elsevier, 2:1405-1418.
- Muhs, D.R. and E.A. Bettis III. 2004. Quaternary loess-paleosol sequences as examples of climate-driven sedimentary extremes, *Geological Society of America Special Paper*; 370:53-74.
- Nahon, D. and R. Trompette. 1982. Origin of Siltstones: glacial grinding versus weathering, *Sedimentology*; 29:25-35.

- Nesbitt, H.W. and G. Markovics. 1997. Weathering of granodioritic crust, long-term storage of elements in weathering profiles, and petrogenesis of siliciclastic sediments, *Geochim. Et Cosmochim. Acta*; 61(8):1653-1670.
- Nicótina, L. Tarboton, D.G., Tesfa, T.K. and A. Rinaldo. 2011. Hydrologic controls on equilibrium soil depths, *Water Resources Research*; 47, Wo4517, 11pp., DOI:10.1029/2010WR009538.
- NOAA. n.d. National Weather Service Forecast Office, *Boise, Id.* Retrieved September 3, 2012. From: <http://www.wrh.noaa.gov/boi/climo.php>
- Noy-Meir, I. 1973. Desert Ecosystems: Environment and Producers, *Annual Review of Ecology and Systematics*; 1973(4):25-51.
- Othberg, K.L. and W.L. Burnham. 1990. Geologic Map of the Lucky Peak Quadrangle, Ada County, Idaho. Idaho Geological Survey Technical Report 90-4 (May, 1990).
- Othberg, K.L., McDaniel, P.A. and M.A. Fosberg. 1997. Soil Development on a Pleistocene Terrace Sequence, Boise Valley, Idaho. *Northwest Science*; 71(4):318-329.
- Othberg, K.L. and V.S. Gillerman. 1994. Field Trip Guide to the Geology of the Boise Valley. Idaho Geological Survey Special Report (October, 1994).
- Othberg, K.L. and L.R. Stanford. 1992. Geologic Map of the Boise Valley and Adjoining Area, Western Snake River Plain, Idaho. Idaho Geological Survey, Geologic Map Series, Scale 1:100,000.
- Poulos, M.J., Flores, A.N., Benner, S.G. and J.L. Pierce. 2012. Hillslope Asymmetry Maps Reveal Widespread, Multi-Scale Organization, *Geophysical Research Letters*; 39, L06406, DOI:10.1029/2012GL051283.
- Pierce, K.L., Fosberg, M.A., Scott, W.E., Lewis, G.C., and Colman, S. M. 1982. Loess deposits of southeastern Idaho--age and correlation of the upper two loess units. In Bonnicksen, Bill, and Breckenridge, R.M., (Eds.), *Cenozoic Geology of Idaho*. Idaho Bureau of Mines and Geology Bulletin, 26:717-725.
- Pierce, K.L., Muhs, D.R., Fosberg, M.A., Mahan, S.A., Rosenbaum, J.G., Licciardi, J.M. and M.J. Pavich. 2011. A loess-paleosol record of climate and glacial history over the past two glacial-interglacial cycles (~150 ka), southern Jackson Hole, Wyoming, *Quaternary Research*; 76(1):119-141.
- Pye, K. 1987. *Aeolian Dust and Dust Deposits*. Academic Press, London, 334 pp.
- Raab, G.A., Bartling, M.H., Stapanian, M.A., Cole, W.H., Tidwell, R.L. and K.A. Cappel. 1990. The Homogenization of Environmental Soil Samples in Bulk. In: Simmons, M. (ed.) *Hazardous Waste Measurements*. Lewis Pub.
- Reheis, M., Honke, J., Lamothe, P. and E. Fisher. 2008. Analytical Results for Deposited Dust Samples from a Two-Year Monitoring Program near Deer Trail, Colorado, USA, 2006-2007. US Geological Survey Open-File Report 2008-1361.

- Reheis, M.C. and R. Kihl. 1995. Dust deposition in southern Nevada and California, 1984-1989: Relations to climate, source area and source lithology, *Journal of Geophysical Research*; 100(5):8893-8918.
- Reynolds, R.L., M. Reheis, J. Yount, and P. Lamothe. 2006. Composition of aeolian dust in natural traps on isolated surface of the central Mojave Desert—Insights to mixing, sources, and nutrient inputs, *J. Arid Environ.*; 66:42–61, DOI:10.1016/j.jaridenv.2005.06.031.
- Riley, K. and B. Stark. 2010. *Granodiorite weathering in Dry Creek Experimental Watershed*. unpublished data.
- Rodriguez-Iturbe, I., Porporato, A., Laio, F. and L. Ridolfi. 2001. Plants in water-controlled ecosystems: active role in hydrologic processes and response to water stress - I. Scope and general outline. *Advances in Water Resources*; 24(7):695-705.
- Rutter, N.W., Ding, Z. and T. Liu. 1996. Long Paleoclimate Records from China, *Geophysica*; 32(1-2):7-34.
- Schumacher, B.A., Shines, K.C., Burton, J.V. and M.L. Papp. 1990. Comparison of soil sample homogenization techniques (EPA 600//X-90/043). Environmental Monitoring Systems laboratory, Las Vegas, NV: U.S. Environmental Protection Agency.
- Smalley, I.J. 1966. The Properties of Glacial Loess and the Formation of Loess Deposits, *Journal of Sedimentary Petrology*; 36(3):669-676.
- Smith, T.J., McNamara, J.P., Flores, A.N., Gribb, M.M., Aishlin, P.S. and S.G. Benner. 2011. Limited soil storage capacity constrains upland benefits of winter snowpack, *Hydrologic Processes*; 25:3858-3865, DOI: 1002/hyp8340.
- Smith, T.J. 2010. Using Soil Moisture Trends Across Topographic Gradients To Examine Controls on Semi-Arid Ecosystem Dynamics. Department of Geosciences, Hydrologic Sciences. Boise, ID, Boise State University. Masters of Science: 219 pp.
- Smith, B.J., Wright, J.S. and W.B. Whaley. 2002. Sources of non-glacial, loess-size quartz silt and the origins of “desert loess”, *Earth Science Reviews*; 59:1-26.
- Sweeney, M.R., Busacca, A.J., Richardson, C.A., Blinnikov, M. and E.V. McDonald. 2004. Glacial anticyclone recorded in Palouse loess of northwestern United States, *Geology*; 32(8):705-708; DOI: 10.1130/G20584.1.
- Sweeney, M.R., Gaylord, D.R. and A.J. Busacca. 2007. Evolution of Eureka Flat: A dust-producing engine of the Palouse loess, USA. *Quaternary International*; 162-163:76-96.
- Taylor, S.R., McLennan, S.M. and M.T. McCullough. 1983. Geochemistry of loess, continental crust composition and crustal model ages. *Geochim. Cosmochim. Acta*; 47(11):1897-1905.

- Tesfa, T.K., Tarboton, D.G., Chandler, D.G. and J.P. McNamara. 2009. Modeling Soil Depth from Topographic and Land Cover Attributes, *Water Resources Research*; 45, W10438, DOI:10.1029/2008WR007474.
- Tijani, M.N., Okunlola, O.A. and A.F. Abimbola. 2006. Lithogenic concentrations of trace metal in soils and saprolites over crystalline basement rocks: A case study from SW Nigeria, *Journal of African Earth Sciences*; 46:427-438.
- USDA. Natural Resource Conservation Service. Web Soil Survey. USDA, Pub . Nov. 2002. Accessed Web. 25 Apr. 2010. <<http://websoilsurvey.nrcs.usda.gov/>>.
- Van Boxel, J. H., Arens, S.M. and P.M. Van Dijk. 1990. Aeolian Processes Across Transverse Dunes I: Modeling the Airflow, *Earth Surface Processes and Landforms*; 24:255-270.
- Walker, P.H., Chartres, C.J. and J. Hutka. 1988. The effect of Aeolian accretions on soil development on granitic rocks in southeastern Australia. I. Soil morphology and particle size distributions, *Australian Journal of Soil Research*; 26:1-16. DOI:10.1071SR9880001.
- White, C.M., Hart, W.K., Bonnicksen, B. and D. Matthews. 2002. Geochemical and Sr-isotopic variations in western Snake River Plain basalts, Idaho. In: Bonnicksen, B., White, C. M. and M. McCurry. (eds) Tectonic and Magmatic Evolution of the Snake River Plain Volcanic Province, *Idaho Geological Survey Bulletin*; 30:329-342.
- Wilkinson, B. H., and B. J. McElroy. 2007. The impact of humans on continental erosion and sedimentation, *Geol. Soc. Am. Bull.*; 119:140–156, DOI:10.1130/B25899.1.
- Williams, C. J. 2005. Characterization of the spatial and temporal controls on soil moisture and streamflow generation in a semi-arid headwater catchment. Department of Geology. Boise, Idaho, Boise State University. Master of Science: 204pp.
- Wood, S.H., and D.M. Clemens, 2002, Geologic and tectonic history of the western Snake River Plain, Idaho and Oregon, In: Bonnicksen, B., White, C.M. and Michael McCurry (eds), Tectonic and Magmatic Evolution of the Snake River Plain Volcanic Province: *Idaho Geological Survey Bulletin*; 30:69-103.
- Wood, S.H. 1994. Seismic Expression and Geological Significance of a Lacustrine Delta in Neogene Deposits of the Western Snake River Plain, Idaho, *AAPG Bulletin*; 78(1):102-121.
- Wood, S. H., and W. L. Burnham. 1987. Geologic framework of the Boise Warm Springs geothermal area, Idaho, in Buess, S.S. (eds), Geological Society of America Centennial Field Guide; 2:117–122.
- Wood, S.H. 1983. Boise, Idaho, geothermal system: Transactions of the Geothermal Resource Council, 7:215-225. In: Bliss, J.D. and P.R. Moyle. 2001. Assessment of the sand and gravel resources of the Lower Boise River Valley Area, Idaho,

Part one: geological framework of the sand and gravel deposits. USGS Open File Report 01-130.

- Wright, J., Smith, B, and B. Whaley. 1998. Mechanisms of loess-sized quartz silt production and their relative effectiveness: laboratory simulations, *Geomorphology*; 23(1):15-34.
- Yaalon, D.H. and E, Ganor. 1973. The Influence of Dust on Soils During the Quaternary, *Soil Science*; 116(3):146-155.
- Yenko M. 2003. Hydrometric and geochemical evidence of streamflow sources in the Upper Dry Creek Experimental Watershed, Southwester Idaho. Master's thesis, Boise State University, Boise, ID

Table 1: Major element data (ICP-MS) for all bulk samples.

Sample	Na %	Na2O wt %	Mg %	MgO wt %	Al %	Al2O3 wt %	Si %	SiO2 wt %	P ppm	P2O5 wt %	K %	K2O wt %	Ca %	CaO wt %	Fe %	FeO wt %	Mn ppm	MnO wt %
LOESS																		
GT-HW21_10-25	2.0	2.7	0.8	1.4	8.1	15.2	31.1	66.5	549	0.1	2.4	2.9	1.1	1.5	3.1	3.9	530	0.1
GT-RR_20-30L	2.0	2.6	0.4	0.7	6.4	12.1	33.0	70.7	345	0.1	2.0	2.5	1.3	1.8	1.9	2.5	551	0.1
GT-RR_30-45L	1.8	2.5	0.9	1.5	8.0	15.0	34.6	74.0	472	0.1	2.1	2.5	1.1	1.6	3.3	4.3	600	0.1
GT-RR_55-70L	2.2	2.9	1.0	1.7	7.6	14.4	33.5	71.6	515	0.1	2.2	2.6	1.5	2.0	3.0	3.8	550	0.1
KB_3-8L	1.5	2.1	0.7	1.2	6.3	11.9	34.5	73.8	707	0.2	1.8	2.1	1.7	2.4	2.7	3.4	966	0.1
KB_8-13L	1.5	2.1	0.7	1.1	6.4	12.1	35.3	75.5	490	0.1	1.8	2.2	1.6	2.2	2.6	3.4	871	0.1
Average	1.8	2.5	0.8	1.3	7.1	13.5	33.7	72.0	512.9	0.1	2.0	2.5	1.4	1.9	2.8	3.6	678.2	0.1
DCEW SOILS																		
LN_0-23	1.5	2.0	0.3	0.5	7.0	13.2	33.5	71.7	394	0.1	1.8	2.2	1.1	1.5	2.0	2.6	513	0.1
LN_23-47	1.6	2.2	0.4	0.6	7.9	14.9	33.2	71.1	382	0.1	2.0	2.4	1.2	1.7	2.3	3.0	524	0.1
LN_47-71	1.7	2.3	0.4	0.6	8.3	15.7	33.9	72.5	318	0.1	2.1	2.6	1.2	1.6	2.4	3.1	518	0.1
LN_71-90	1.6	2.1	0.3	0.4	7.8	14.8	34.4	73.7	261	0.1	2.2	2.6	0.9	1.3	1.8	2.3	366	0.0
LN_94-117	1.3	1.8	0.2	0.3	7.9	15.0	34.8	74.3	187	0.0	2.4	2.9	0.7	1.0	1.4	1.9	171	0.0
LS_0-10	2.4	3.2	0.2	0.4	7.3	13.9	35.1	75.2	283	0.1	1.9	2.3	1.6	2.2	1.3	1.6	247	0.0
LS_21-31	2.4	3.3	0.3	0.5	7.7	14.6	34.5	73.8	292	0.1	2.3	2.7	1.6	2.2	1.8	2.4	496	0.1
MLN_0-10	1.9	2.6	0.4	0.6	6.8	12.9	30.6	65.5	413	0.1	2.0	2.4	1.4	2.0	1.6	2.1	402	0.1
MLN_45-55	2.1	2.8	0.4	0.7	7.4	14.0	30.8	65.8	431	0.1	1.9	2.3	1.4	1.9	1.9	2.4	413	0.1
MLN_85-95	2.1	2.9	0.4	0.7	7.6	14.4	31.4	67.2	342	0.1	2.1	2.5	1.4	1.9	1.9	2.4	413	0.1
MLN_125-135	2.5	3.3	0.4	0.6	7.7	14.5	33.4	71.5	236	0.1	2.0	2.4	1.5	2.1	1.7	2.1	284	0.0
MLS_0-10	2.4	3.3	0.4	0.6	8.6	16.2	32.4	69.2	671	0.2	2.0	2.4	1.7	2.3	2.1	2.7	421	0.1
MLS_10-25	2.5	3.4	0.4	0.6	9.0	17.1	33.2	71.0	622	0.1	2.1	2.5	1.6	2.2	2.2	2.9	426	0.1
MLS_30-40	2.4	3.2	0.3	0.4	8.6	16.3	32.6	69.7	666	0.2	2.0	2.4	1.4	2.0	2.0	2.6	422	0.1
MLS_0-5L1	2.5	3.4	0.3	0.6	8.6	16.3	34.7	74.3	598	0.1	2.0	2.4	1.7	2.4	2.0	2.6	411	0.1
MLS_0-5L2	2.3	3.1	0.3	0.5	8.2	15.5	32.3	69.2	543	0.1	2.0	2.4	1.6	2.3	1.9	2.4	386	0.0
MHN_0-10	1.7	2.3	0.3	0.5	6.7	12.6	29.6	63.3	742	0.2	2.0	2.5	1.2	1.6	1.8	2.3	901	0.1
MHN_15-25	2.1	2.8	0.4	0.7	8.3	15.7	34.4	73.7	955	0.2	2.4	2.8	1.2	1.7	2.4	3.1	1006	0.1
MHN_45-55	2.2	2.9	0.3	0.5	8.4	15.8	34.6	74.1	557	0.1	2.4	2.9	0.9	1.3	2.2	2.8	463	0.1
MHN_100-110	2.1	2.8	0.3	0.5	7.9	14.9	33.2	70.9	206	0.0	2.4	2.9	0.8	1.2	2.1	2.7	276	0.0
MHS_0-10	3.0	4.0	0.4	0.6	8.8	16.6	34.6	74.0	695	0.2	2.1	2.5	1.6	2.3	1.8	2.3	425	0.1
MHS_30-40	2.9	3.9	0.4	0.7	9.2	17.4	33.5	71.6	530	0.1	2.0	2.4	1.6	2.2	1.9	2.4	441	0.1
MHS_55-65	2.8	3.7	0.4	0.7	8.7	16.5	32.0	68.5	616	0.1	2.0	2.5	1.6	2.2	1.9	2.5	439	0.1
MHS_80-90	2.9	3.9	0.3	0.5	8.5	16.1	34.4	73.5	457	0.1	2.2	2.6	1.6	2.3	1.5	1.9	323	0.0
HN_0-10	1.9	2.6	0.5	0.8	8.3	15.6	31.9	68.2	1486	0.3	2.3	2.8	1.4	2.0	2.4	3.1	1337	0.2
HN_20-35	2.0	2.7	0.4	0.6	8.3	15.7	29.5	63.2	413	0.1	2.4	2.9	1.0	1.5	2.2	2.8	714	0.1
HN_50-65	2.5	3.4	0.4	0.6	8.9	16.9	35.9	76.7	198	0.0	2.5	3.0	1.1	1.6	1.8	2.4	200	0.0
HS_0-10	1.8	2.5	0.4	0.6	8.2	15.5	32.0	68.4	1125	0.3	2.4	2.8	1.2	1.7	2.3	3.0	950	0.1
HS_20-40	1.9	2.5	0.3	0.5	8.1	15.3	33.2	71.1	733	0.2	2.6	3.1	0.9	1.3	2.1	2.7	556	0.1
HS_55-70	2.0	2.7	0.3	0.5	8.5	16.1	36.0	77.1	639	0.1	2.8	3.4	0.9	1.3	2.0	2.6	487	0.1
Average	2.2	2.9	0.3	0.6	8.1	15.3	33.2	71.0	533.0	0.1	2.2	2.6	1.3	1.8	2.0	2.5	497.7	0.1
BEDROCK																		
MLN_130G	2.3	3.1	0.2	0.3	7.3	13.8	34.2	73.2	132	0.0	3.0	3.7	1.1	1.5	0.7	1.0	155	0.0
MHN_130G	2.8	3.8	0.2	0.3	8.2	15.6	37.2	79.6	301	0.1	2.6	3.1	0.6	0.8	1.4	1.8	304	0.0
HN_50-65G	3.0	4.1	0.3	0.4	8.4	15.9	38.7	82.7	139	0.0	2.6	3.1	1.3	1.8	1.2	1.5	193	0.0
HS_100-110G	2.6	3.5	0.4	0.6	7.9	14.9	35.7	76.4	519	0.1	2.1	2.6	1.8	2.5	1.7	2.2	305	0.0
RR-C	2.7	3.7	0.3	0.6	8.1	15.2	36.4	77.8	420	0.1	2.1	2.6	1.9	2.6	1.7	2.1	270	0.0
RR-G	2.7	3.6	0.4	0.6	8.1	15.4	35.5	75.8	444	0.1	2.7	3.3	1.8	2.5	1.4	1.9	272	0.0
8S-G	2.7	3.7	0.2	0.3	9.0	17.0	34.1	73.0	98	0.0	2.5	3.0	1.1	1.6	1.3	1.6	284	0.0
Average	2.7	3.6	0.3	0.4	8.1	15.4	36.0	76.9	293.1	0.1	2.5	3.0	1.4	1.9	1.3	1.7	254.6	0.0
BASALTS																		
BA-HW21-A	1.7	2.3	4.3	7.2	7.4	14.0	23.1	49.4	3197	0.7	0.5	0.6	6.8	9.5	12.4	15.9	1764	0.2
BA-HW21-B	1.9	2.6	4.7	7.8	8.0	15.2	23.1	49.3	1654	0.4	0.9	1.1	7.0	9.8	9.8	12.6	1475	0.2
BA-CR	1.7	2.3	3.3	5.4	8.4	15.8	22.5	48.1	1233	0.3	0.5	0.6	7.1	9.9	10.0	12.9	1289	0.2
BA-FHL	1.9	2.6	4.3	7.1	8.1	15.3	23.6	50.5	975	0.2	0.4	0.5	7.6	10.6	9.5	12.2	1311	0.2
BA-FHM	1.6	2.2	3.9	6.5	8.2	15.4	23.2	49.6	1321	0.3	0.3	0.3	8.1	11.3	9.1	11.8	1474	0.2
BA-FHH	1.8	2.4	4.8	7.9	8.0	15.0	22.6	48.4	820	0.2	0.4	0.5	7.0	9.8	8.3	10.7	1310	0.2
Average	1.8	2.4	4.2	7.0	8.0	15.1	23.0	49.2	1533.5	0.4	0.5	0.6	7.3	10.2	9.9	12.7	1437.2	0.2

Table 2: Minor and trace element data (ICP-MS) for all bulk samples.

All data reported in ppm. (N.D. = non-detectable; N.R. = not reported).

Sample	Sc	Ti	V	Cr	Co	Ni	Cu	Zn	Rb	Sr	Y	Zr	Nb	Cs	Ba	Hf	Ta	Pb	Th	U
LOESS																				
GT-HW21_10-25	9	3594	47	38	8	27	38	80	101	338	26	354	34	4	1004	9.6	2.2	23.0	17.2	3.7
GT-RR_20-30L	6	3472	35	31	8	11	16	49	80	316	23	331	25	3	865	8.8	1.7	19.5	13.2	3.1
GT-RR_30-45L	11	3811	53	42	10	20	47	88	95	296	28	320	29	4	803	8.7	1.9	20.7	15.3	3.9
GT-RR_55-70L	9	3671	64	40	9	19	45	74	93	346	27	337	31	4	1132	9.1	2.1	20.7	15.3	4.3
KB_3-8L	9	4551	57	44	16	18	23	60	66	286	28	346	17	3	761	8.8	1.1	16.3	9.0	2.6
KB_8-13L	9	4622	57	44	15	19	25	59	71	285	28	351	18	3	757	8.9	1.2	17.5	9.3	2.6
Average	9	3954	52	40	11	19	32	68	84	311	26	340	26	4	887	9	2	20	13	3
DCEW SOILS																				
LN_0-23	6	2770	27	17	7	8	19	72	70	316	14	192	11	4	1201	5.2	0.6	21.2	9.3	2.2
LN_23-47	7	3304	35	21	8	10	16	75	79	339	17	212	13	4	1329	5.6	0.7	20.2	10.9	2.5
LN_47-71	7	3499	36	22	8	10	17	75	84	354	19	234	14	4	1381	6.1	0.8	21.4	11.6	2.7
LN_71-90	5	2631	24	13	5	7	55	63	77	333	12	196	11	3	1438	5.1	0.6	21.3	10.0	2.2
LN_94-117	4	1925	12	5	2	3	6	58	77	298	10	157	8	3	1566	4.2	0.4	21.5	9.7	1.8
LS_0-10	3	1639	3	2	7	1	3	63	61	505	10	164	7	1	1383	4.3	0.3	19.0	9.7	1.8
LS_21-31	4	1667	5	1	2	1	2	76	68	521	9	159	7	2	1747	4.3	0.3	20.7	9.2	2.1
MLN_0-10	4	2222	14	9	4	5	13	86	79	439	10	166	9	3	1619	4.4	0.7	17.1	7.7	1.8
MLN_45-55	5	2594	20	11	4	6	11	76	83	439	11	179	10	3	1391	4.7	0.8	15.0	8.7	2.0
MLN_85-95	5	2564	19	10	4	5	9	77	88	453	11	184	10	3	1643	4.8	0.8	16.1	9.4	2.0
MLN_125-135	4	2179	10	N.R.	4	7	47	81	84	495	8	176	9	2	1426	4.6	0.7	15.0	7.9	1.5
MLS_0-10	6	2796	16	7	3	3	9	114	81	465	14	223	11	3	1189	5.8	0.6	19.8	14.7	2.0
MLS_10-25	6	2843	17	6	4	3	5	107	83	463	15	212	12	4	1215	5.5	0.7	19.9	14.5	2.1
MLS_30-40	5	2382	12	3	3	2	12	96	74	428	13	185	10	6	1104	4.8	0.6	19.8	12.9	1.8
MLS_0-5L1	6	2687	14	6	5	3	7	103	77	480	14	210	11	3	1248	5.4	0.6	19.8	14.3	1.9
MLS_0-5L2	5	2449	12	5	3	3	7	98	73	462	12	184	10	3	1335	4.8	0.5	19.8	12.3	1.7
MHN_0-10	4	2393	15	11	4	7	24	121	71	307	12	183	12	3	1322	4.7	0.7	17.8	12.9	1.7
MHN_15-25	7	3231	26	17	6	11	21	155	87	355	16	230	16	4	1421	5.9	0.9	18.9	12.1	2.1
MHN_45-55	6	3131	25	15	5	9	11	83	90	349	14	241	16	3	1285	6.1	0.9	19.2	12.0	2.1
MHN_100-110	5	3061	25	15	5	6	8	69	94	330	10	230	17	3	1184	5.9	0.9	19.0	12.6	2.0
MHS_0-10	5	2349	12	5	3	3	6	96	102	536	10	189	9	3	1081	4.8	1.1	19.0	10.5	2.1
MHS_30-40	5	2456	14	6	3	3	11	176	104	516	11	202	10	3	1019	5.2	1.2	18.1	10.8	2.3
MHS_55-65	5	2607	13	4	2	2	6	92	103	503	11	199	10	3	1062	5.0	1.3	17.6	12.4	2.4
MHS_80-90	4	2139	7	5	1	1	3	67	94	565	7	153	9	2	1259	3.9	1.2	18.4	8.9	1.8
HN_0-10	7	3053	33	19	8	13	25	193	117	333	20	185	13	5	1201	5.0	1.1	26.1	16.2	3.0
HN_20-35	5	2660	23	14	6	15	17	137	125	293	21	198	13	5	1159	5.3	1.1	27.8	21.4	3.7
HN_50-65	5	2531	19	11	3	6	10	80	135	330	22	215	14	4	954	5.8	1.3	28.7	31.0	4.4
HS_0-10	6	2891	19	9	5	4	13	129	99	406	17	202	12	4	1523	5.4	1.1	21.8	12.5	2.3
HS_20-40	6	2661	14	6	4	3	9	89	102	374	15	207	12	3	1533	5.4	1.0	20.2	12.1	2.3
HS_55-70	6	2722	14	5	4	3	8	82	107	406	15	224	12	3	1820	5.8	1.0	20.9	12.1	2.4
Average	5	2601	18	10	4	5	14	96	89	413	13	196	11	3	1335	5	1	20	12	2
BEDROCK																				
MLN_130G	2	1464	N.D.	1	1	0	5	45	97	471	6	107	6	2	2038	2.8	0.6	17.2	7.1	2.1
MHN_130G	4	2044	1	1	2	3	3	55	95	394	18	174	12	2	1263	4.2	0.6	17.1	10.9	2.3
HN_50-65G	3	1629	3	1	2	21	6	77	119	386	16	180	10	2	1143	4.8	0.9	26.5	20.1	2.9
HS_100-110G	4	2357	6	1	2	1	31	87	86	639	12	193	10	2	1763	5.0	1.0	17.2	17.7	1.5
RR-C	4	2059	4	1	1	0	1	83	73	623	8	201	12	1	1738	5.4	0.6	19.2	12.4	1.0
RR-G	4	2123	5	1	2	0	9	77	82	660	7	169	13	1	2693	4.5	0.8	21.9	5.7	0.9
8S-G	3	1369	N.D.	2	1	2	5	73	103	456	16	120	20	3	1110	3.0	1.6	17.7	8.5	4.4
Average	3	1864	4	1	2	4	9	71	93	518	12	163	12	2	1678	4	1	20	12	2
BASALTS																				
BA-HW21-A	32	20060	314	142	57	67	32	169	7	336	43	282	29	0	435	5.9	1.6	4.8	1.1	0.3
BA-HW21-B	31	12700	233	192	55	117	65	112	22	337	30	166	26	0	434	3.8	1.5	3.0	1.6	0.3
BA-CR	30	16140	271	102	49	79	15	126	9	284	34	154	14	1	339	4.0	0.9	3.1	0.6	0.2
BA-FHL	29	11810	284	171	57	152	57	115	6	475	47	125	11	0	271	3.1	0.6	2.4	0.9	0.2
BA-FHM	37	10380	264	297	53	89	62	107	4	264	35	115	12	0	670	2.8	0.6	3.0	0.8	0.3
BA-FHH	29	11270	267	160	51	142	55	111	5	435	25	125	11	0	162	3.2	0.6	2.3	0.9	0.2
Average	31	13727	272	177	54	108	47	123	9	355	35	161	17	0	385	4	1	3	1	0

Table 3: Rare earth element data (ICP-MS) for all bulk samples.

All data reported in ppm.

	La	Ce	Pr	Nd	Sm	Eu	Gd	Th	Dy	Ho	Er	Tm	Yb	Lu
LOESS														
GT-HW21_10-25	46.4	85.6	9.9	35.1	6.7	1.4	5.6	0.8	4.8	1.0	2.6	0.4	2.6	0.4
GT-RR_20-30L	38.4	73.4	8.3	29.9	5.7	1.2	4.8	0.7	4.1	0.8	2.3	0.3	2.2	0.4
GT-RR_30-45L	41.4	77.9	9.1	32.8	6.3	1.4	5.5	0.8	4.9	1.0	2.8	0.4	2.7	0.4
GT-RR_55-70L	43.5	80.8	9.4	33.7	6.5	1.4	5.5	0.8	4.8	1.0	2.7	0.4	2.6	0.4
KB_3-8L	34.8	76.9	7.9	29.5	6.0	1.4	5.4	0.9	5.1	1.0	2.8	0.4	2.8	0.4
KB_8-13L	34.3	73.1	7.8	28.8	5.8	1.4	5.2	0.8	5.0	1.0	2.9	0.4	2.7	0.4
Average	39.8	77.9	8.7	31.7	6.2	1.4	5.3	0.8	4.8	1.0	2.7	0.4	2.6	0.4
DCEW SOILS														
LN_0-23	32.8	65.4	7.3	26.1	4.8	1.1	3.7	0.5	2.8	0.5	1.5	0.2	1.4	0.2
LN_23-47	39.0	75.8	8.5	30.3	5.7	1.2	4.3	0.6	3.3	0.6	1.7	0.2	1.5	0.2
LN_47-71	41.5	80.6	9.0	32.5	6.0	1.3	4.7	0.7	3.5	0.7	1.9	0.3	1.8	0.3
LN_71-90	37.1	71.6	8.1	28.6	5.2	1.2	3.8	0.5	2.5	0.5	1.2	0.2	1.1	0.2
LN_94-117	36.5	68.7	8.0	27.8	4.9	1.1	3.5	0.4	2.0	0.4	0.9	0.1	0.8	0.1
LS_0-10	36.9	69.2	7.9	28.1	4.9	1.1	3.5	0.4	2.1	0.4	1.0	0.1	0.9	0.1
LS_21-31	35.3	66.4	7.6	26.8	4.7	1.2	3.3	0.4	1.9	0.3	0.8	0.1	0.7	0.1
MLN_0-10	29.9	53.8	6.3	22.0	3.8	1.0	2.8	0.4	1.9	0.4	1.0	0.1	0.9	0.1
MLN_45-55	33.8	61.5	7.1	24.9	4.2	1.0	3.2	0.4	2.2	0.4	1.1	0.1	1.0	0.2
MLN_85-95	36.1	66.2	7.6	26.7	4.5	1.1	3.3	0.4	2.2	0.4	1.1	0.1	1.0	0.2
MLN_125-135	30.4	55.2	6.4	22.5	3.8	0.9	2.7	0.3	1.8	0.3	0.8	0.1	0.7	0.1
MLS_0-10	56.3	104.3	12.0	42.3	7.4	1.3	5.2	0.6	3.0	0.5	1.3	0.2	1.3	0.2
MLS_10-25	56.0	104.0	12.0	42.2	7.3	1.3	5.2	0.7	3.2	0.5	1.4	0.2	1.3	0.2
MLS_30-40	48.6	91.3	10.4	37.0	6.7	1.2	4.8	0.6	2.9	0.5	1.2	0.2	1.2	0.2
MLS_0-5L1	54.9	102.1	11.8	41.2	7.2	1.3	5.1	0.6	2.9	0.5	1.3	0.2	1.2	0.2
MLS_0-5L2	47.6	87.8	10.1	35.5	6.2	1.2	4.4	0.5	2.5	0.4	1.1	0.2	1.1	0.2
MHN_0-10	45.1	81.1	9.0	30.3	5.0	0.8	3.6	0.5	2.3	0.4	1.1	0.2	1.0	0.2
MHN_15-25	43.4	77.7	8.6	29.5	5.2	1.1	4.0	0.5	2.9	0.5	1.5	0.2	1.4	0.2
MHN_45-55	43.0	76.7	8.5	28.7	5.0	1.0	3.7	0.5	2.6	0.5	1.3	0.2	1.2	0.2
MHN_100-110	41.7	76.4	8.1	27.4	4.5	0.9	3.1	0.4	2.1	0.4	1.1	0.2	1.0	0.2
MHS_0-10	38.8	71.2	8.3	29.5	5.1	1.2	3.6	0.4	2.0	0.4	1.0	0.2	1.4	0.2
MHS_30-40	39.9	73.3	8.5	30.4	5.3	1.2	3.7	0.4	2.1	0.4	1.0	0.2	1.4	0.2
MHS_55-65	44.6	82.6	9.5	33.5	5.8	1.2	4.0	0.5	2.2	0.4	1.0	0.2	1.4	0.2
MHS_80-90	32.5	59.4	6.9	24.1	4.1	1.1	2.7	0.4	1.4	0.3	0.7	0.2	0.9	0.2
HN_0-10	38.3	77.7	8.5	30.6	6.3	0.9	5.1	0.7	3.8	0.7	1.9	0.3	1.7	0.3
HN_20-35	48.0	96.6	10.9	39.4	8.1	1.0	6.4	0.9	4.4	0.8	2.0	0.3	1.8	0.3
HN_50-65	60.1	119.5	13.9	50.0	10.3	0.8	7.6	1.0	4.7	0.8	2.0	0.3	1.8	0.3
HS_0-10	39.1	69.8	8.0	28.2	5.3	1.3	4.2	0.6	3.2	0.6	1.6	0.2	1.4	0.2
HS_20-40	35.9	64.8	7.5	26.2	4.9	1.2	3.8	0.5	2.9	0.5	1.5	0.2	1.4	0.2
HS_55-70	37.0	65.8	7.7	26.8	4.9	1.3	3.8	0.5	2.9	0.5	1.5	0.2	1.3	0.2
Average	41.3	77.2	8.8	31.0	5.6	1.1	4.1	0.5	2.7	0.5	1.3	0.2	1.2	0.2
BEDROCK														
MLN_130G	26.1	44.7	5.5	19.1	3.2	1.0	2.2	0.3	1.3	0.2	0.6	0.1	0.4	0.1
MHN_130G	48.8	87.3	9.7	32.6	5.5	0.9	4.1	0.6	3.2	0.6	1.8	0.3	1.8	0.3
HN_50-65G	39.3	77.2	9.1	32.8	6.9	0.8	5.2	0.7	3.3	0.6	1.4	0.2	1.3	0.2
HS_100-110G	41.8	77.8	8.7	30.1	5.1	1.3	3.6	0.5	2.4	0.4	1.1	0.1	0.9	0.1
RR-C	38.8	69.0	8.1	28.7	5.0	1.2	3.4	0.4	1.8	0.3	0.8	0.1	0.6	0.1
RR-G	23.8	43.1	4.8	16.7	2.8	1.3	2.1	0.3	1.4	0.3	0.7	0.1	0.6	0.1
8S-G	28.2	57.4	5.5	18.2	3.3	0.8	2.6	0.4	2.5	0.5	1.4	0.2	1.3	0.2
Average	35.2	65.2	7.3	25.5	4.5	1.0	3.3	0.4	2.3	0.4	1.1	0.2	1.0	0.2
BASALTS														
BA-HW21-A	32.4	68.7	8.8	38.1	8.9	3.2	9.3	1.4	8.6	1.6	4.3	0.6	3.5	0.5
BA-HW21-B	21.0	42.4	5.6	24.0	5.7	2.1	5.9	1.0	5.9	1.2	3.1	0.4	2.6	0.4
BA-CR	16.3	36.6	5.2	23.6	6.3	2.3	6.7	1.1	6.9	1.4	3.6	0.5	3.1	0.4
BA-FHL	24.1	32.9	6.2	28.7	7.2	2.7	8.3	1.2	7.2	1.4	3.6	0.4	2.7	0.4
BA-FHM	18.2	30.6	4.6	20.7	5.1	1.8	6.0	1.0	6.2	1.3	3.4	0.5	3.0	0.4
BA-FHH	12.7	29.3	4.2	19.4	5.2	1.9	5.5	0.9	5.3	1.0	2.6	0.3	2.0	0.3
Average	20.8	40.1	5.8	25.7	6.4	2.3	6.9	1.1	6.7	1.3	3.4	0.5	2.8	0.4

Table 4: Chemical loess fraction estimates for Dry Creek soils

Site	Depth (cm bgs)	Chemical Loess Fraction (CLF)	Site Averaged CLF
LN	0-23	0.50	0.44
	23-47	0.60	
	47-71	0.63	
	71-90	0.37	
	94-117	0.12	
MLN	0-10	0.22	0.25
	45-55	0.29	
	85-95	0.29	
	125-135	0.20	
MHN	0-10	0.27	0.37
	15-25	0.46	
	45-55	0.39	
	100-110	0.38	
HN	0-10	0.59	0.43
	20-35	0.46	
	50-65	0.24	
<i>Average CLF of north Facing Soils</i>			<i>0.38</i>
LS	0-10	0.19	0.11
	21-31	0.02	
MLS	0-10	0.20	0.17
	10-25	0.21	
	30-40	0.11	
MHS	0-10	0.15	0.12
	30-40	0.15	
	55-65	0.12	
	80-90	0.04	
HS	0-10	0.29	0.23
	20-40	0.21	
	55-70	0.20	
<i>Average CLF of south Facing Soils</i>			<i>0.16</i>
<i>Average CLF of all Dry Creek Soils</i>			<i>0.28</i>

Table 5: Chemical loess fraction versus elevation.

No consistent trends are apparent for estimated loess fraction as a function of elevation.

Paired Sites	(LN,LS)	(MLN,MLS)	(MHN,MHS)	(HN,HS)
Average Elevation (m)	1130	1293	1465	1824
Avg Loess Fraction	0.35	0.22	0.25	0.33
Min Loess Fraction	0.02	0.11	0.04	0.20
Max Loess Fraction	0.63	0.29	0.46	0.59
Standard Deviation	0.24	0.06	0.15	0.16

Table 6: Summary of the no-dust scenario exercise.

Removal of silt (based on estimated chemical loess fractions) from soils in their current classification would result in primarily sandy soils, and an average of 48% reduction in soil water storage capacity.

Site	Current Soil Class	Current Storage Depth (cm)	Adjusted Soil Class	Adjusted Storage Depth (cm)	Lost Storage (cm)	Lost Storage (%)
LN	sandy loam	10.6	sandy loam	10.6	0.0	0
MLN	sandy loam	14.8	sand	6.1	8.7	59
MHN	sandy loam	15.6	sand	6.4	9.2	59
HN	sandy loam	11.2	sand	4.6	6.6	59
LS	loamy sand	4.4	sand	2.4	2.0	46
MLS	loamy sand	5.7	sand	2.7	3.0	53
MHS	loamy sand	11.4	sand	5.3	6.1	53
HS	loamy sand	11.7	sand	5.1	6.6	56
Average					5.3	48

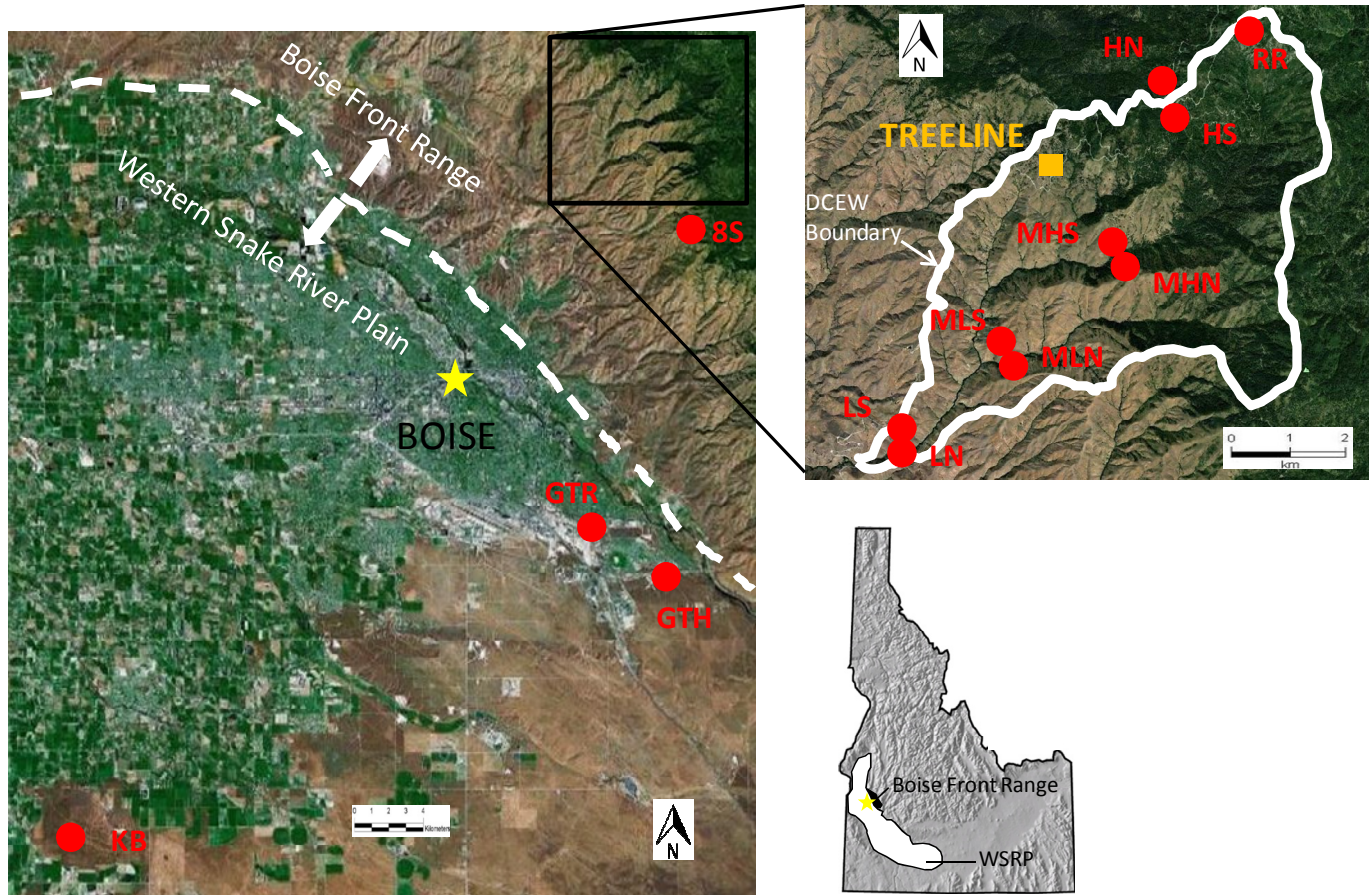


Figure 1: Map of the study area.

Red circles show sampling locations. Loess samples taken from KB, GTR, and GTH sites (n=6); DCEW soil samples taken from HN/HS, MHN/MHS, MLN/MLS, and LN/LS sites (n=30); bedrock samples taken from soil pits, 8S, and RR sites (n=7).

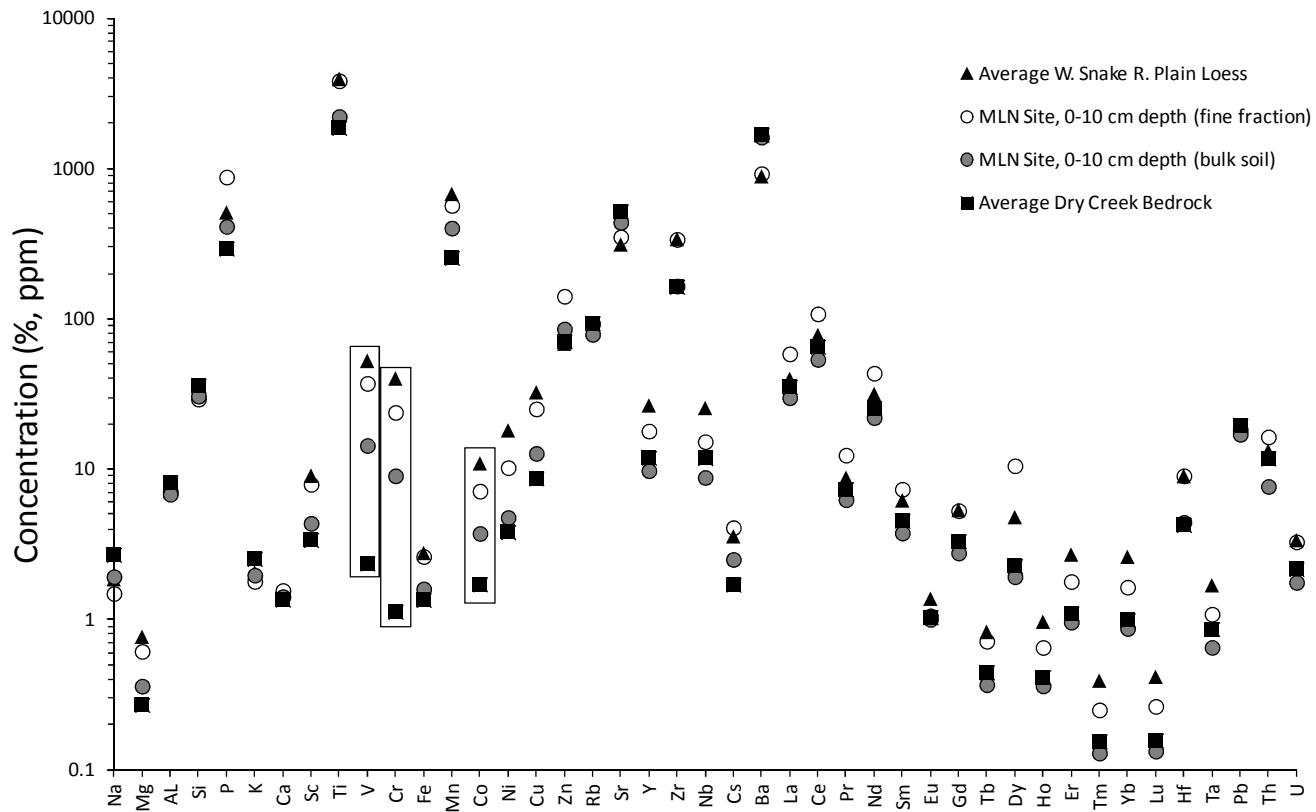


Figure 2: Elemental concentrations in average bedrock, average loess, selected bulk soil MLN, 0-10 cm depth), and associated soil fine fractions (<75μm).

Trace elements V, Cr, and Co (boxed) show the greatest separation between end-members and soils with concentrations in the fine fractions closer to concentrations in the loess that in associated bulk soil.

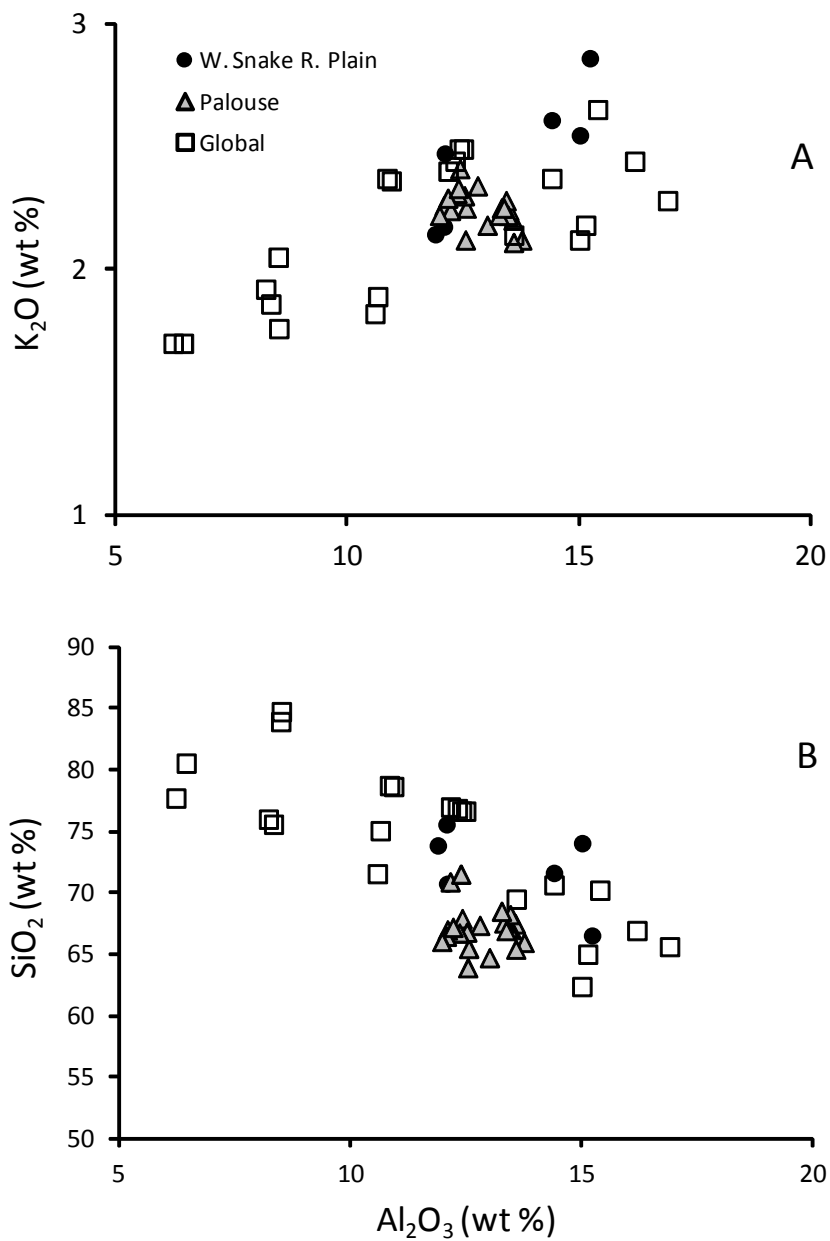


Figure 3: Major element composition of the WSRP loess.

Also included in the plot is data from Washington Palouse loess (Sweeney *et al.*, 2007) and global loess (Gallet *et al.*, 1998). Major element composition of WSRP loess appears similar to loess found in other regions.

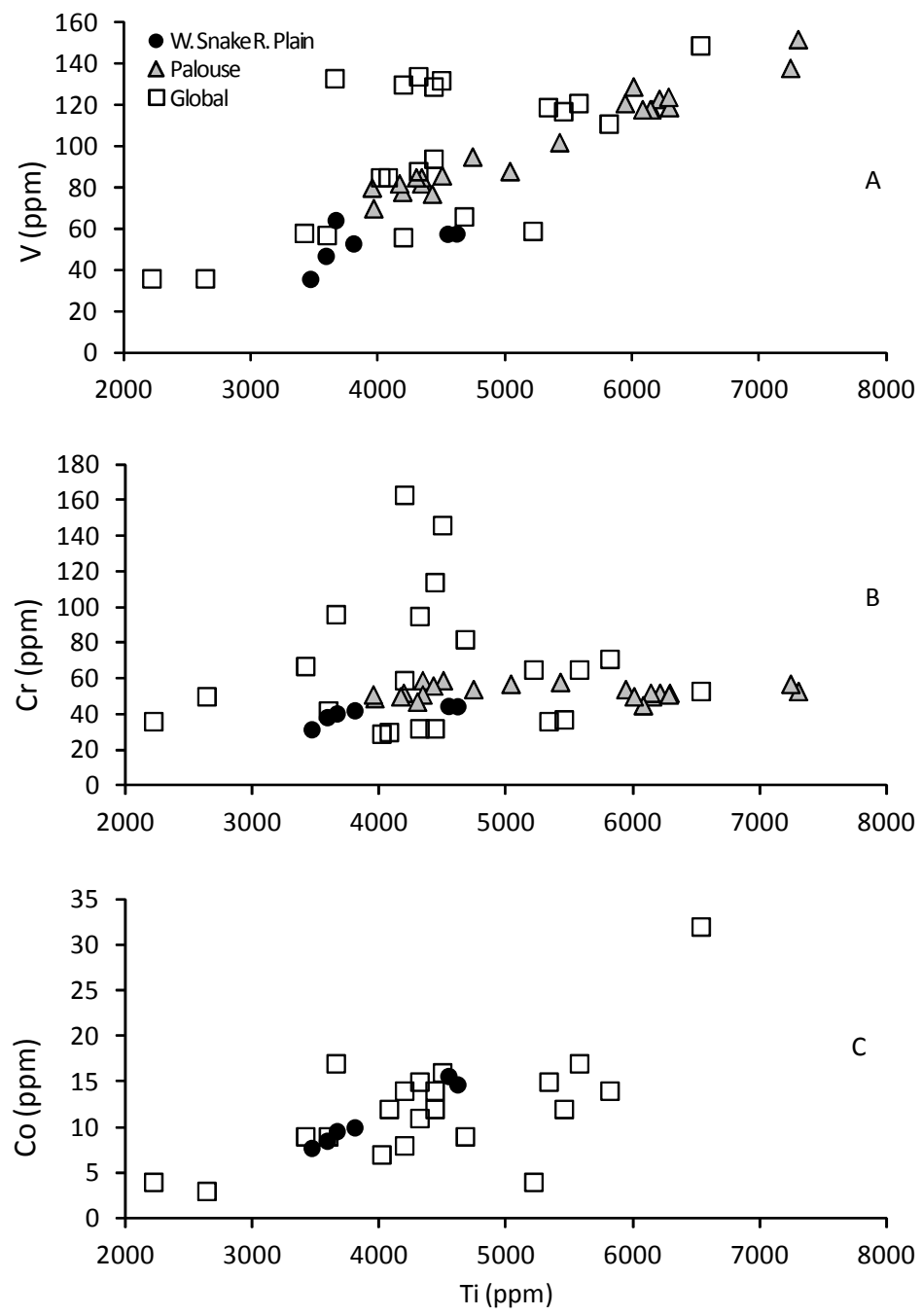


Figure 4: Trace element composition of WSRP loess.

Also included in the plot is data from Washington Palouse loess (Sweeney *et al.*, 2007) and global loess (Gallet *et al.*, 1998). No Co data was available for the Palouse Loess.

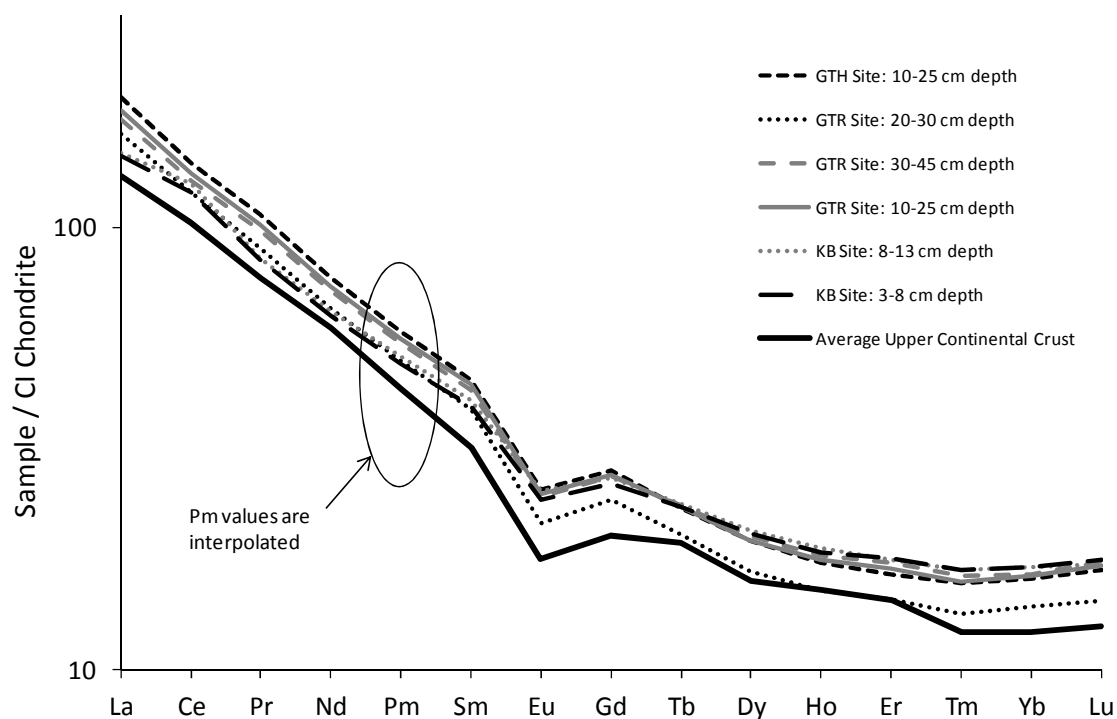


Figure 5: Rare Earth element composition of WSRP loess.

WSRP loess sampled from GTH, GTR and KB locations shown in Figure 1. Estimated REE composition of the average upper continental crust (Gallet *et al.*, 1998) is included for comparison. All data is normalized to CI chondrite data from McDonough and Sun (1995).

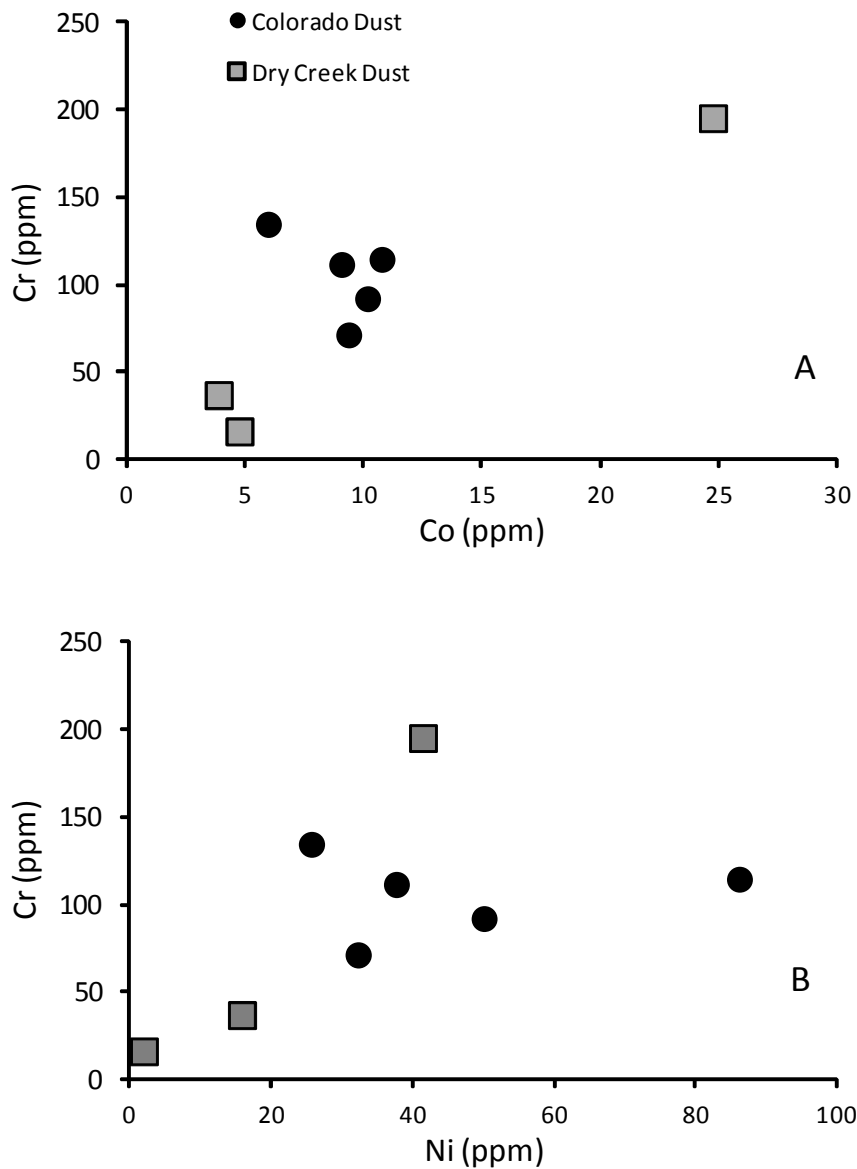


Figure 6: Select trace element compositions of snowpack dust in the DCEW. Data is compared here to dust collected in dust traps in Colorado (Reheis *et al.*, 2008).

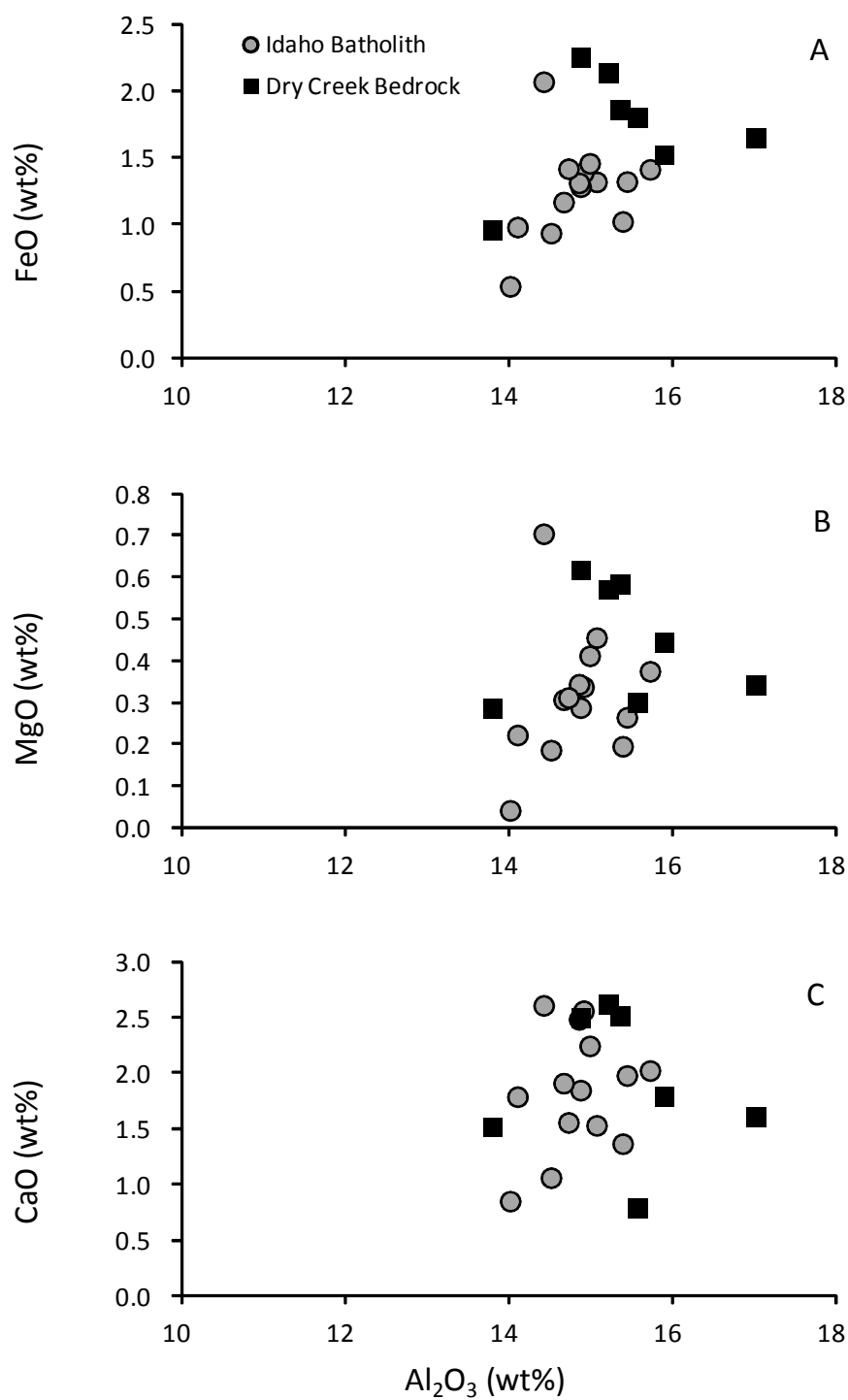


Figure 7: Major element composition of DCEW bedrock.

Data from throughout the Atlanta Lobe of the Idaho Batholith (Gaschnig *et al.*, 2011) is included for comparison.

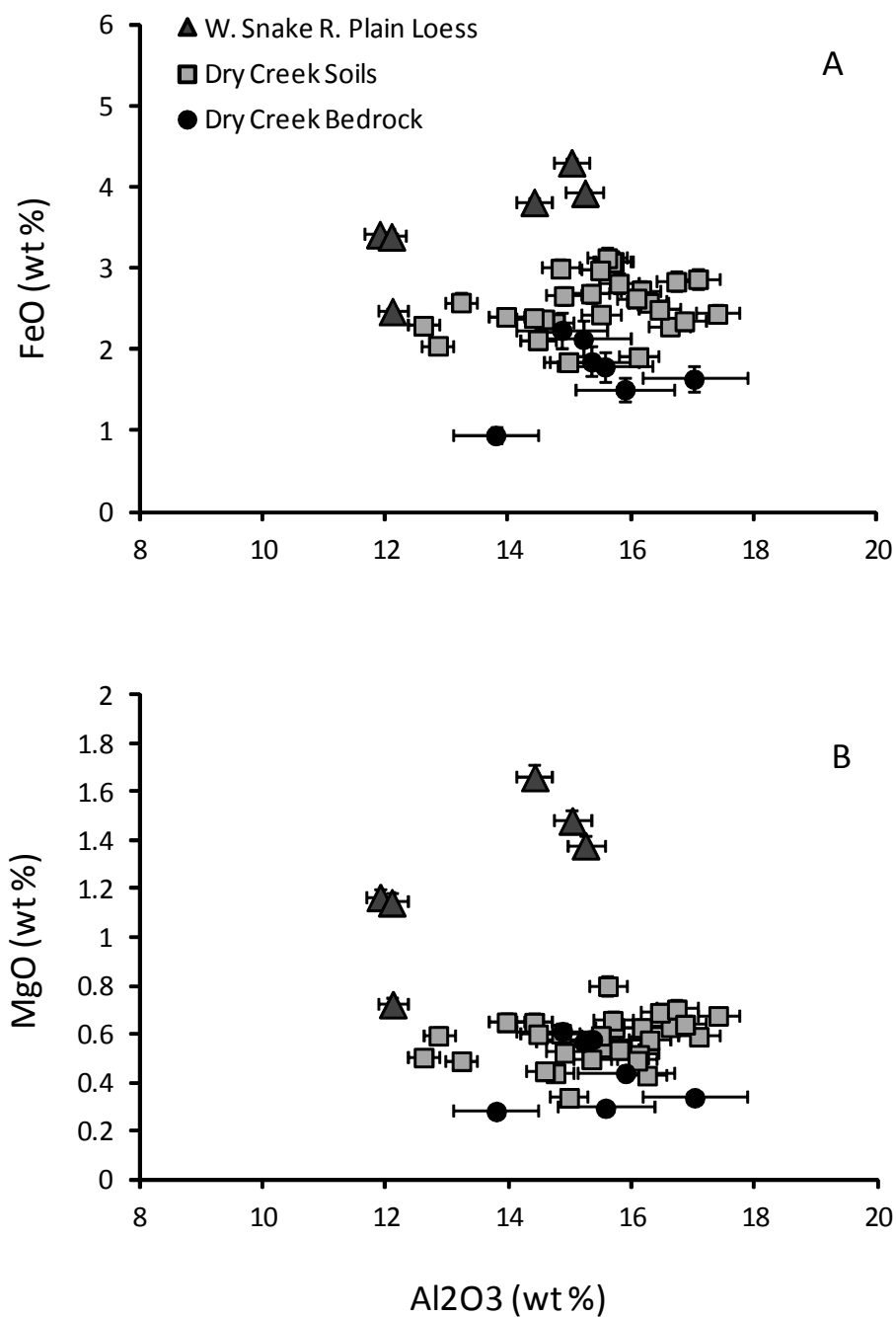


Figure 8: Major element comparisons of DCEW soil to loess and bedrock.

A weak trend of mixing is evidenced by soil compositions lying between loess and bedrock in major element compositional space. Error bars represent the quadrature sum of one standard deviation of procedural and machine variabilities.

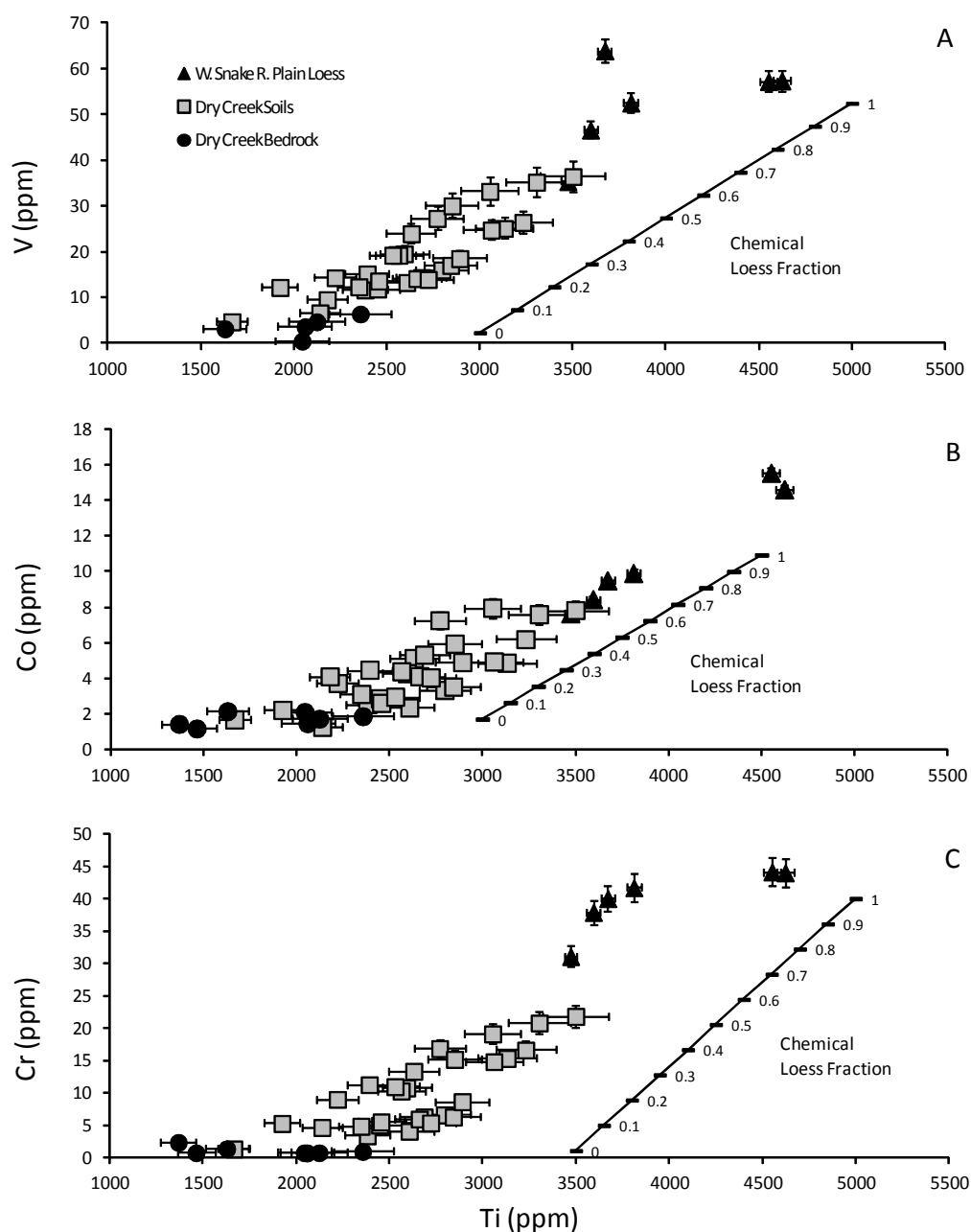


Figure 9: Trace element comparison of DCEW soils to loess and bedrock.

Figure 9 (A-C) shows data for all bedrock, soils, and loess. Soils generally plot between loess and bedrock. Scales for chemical loess fraction are based on mixing model calculations for each element using the average of end-member populations (the chemical loess fractions described in text represent the average of these three models). Error bars represent the quadrature sum of one standard deviation of procedural and machine variabilities.

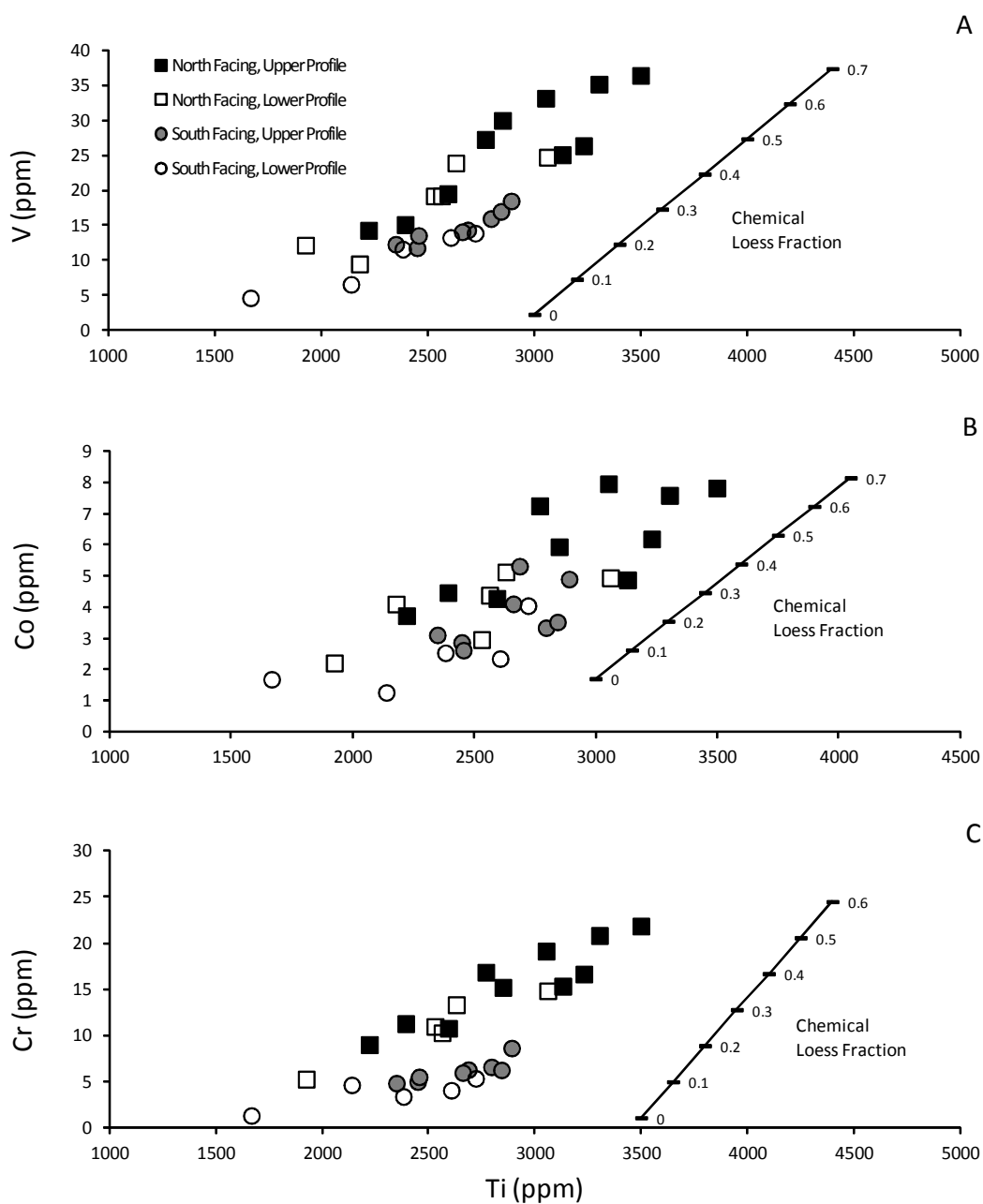


Figure 10: Trace element comparison of DCEW soil classes.

Figure 10 (A-C) shows soils only, broken into four classes; upper profile on north slopes, lower profile on north slopes, upper profile on south slopes, and lower profile on south slopes. Soils show trends of elevated trace element concentrations in the upper profile and on north slopes. Scales for chemical loess fraction are based on mixing model calculations for each element using the average of end-member populations (the chemical loess fractions described in text represent the average of these three models).

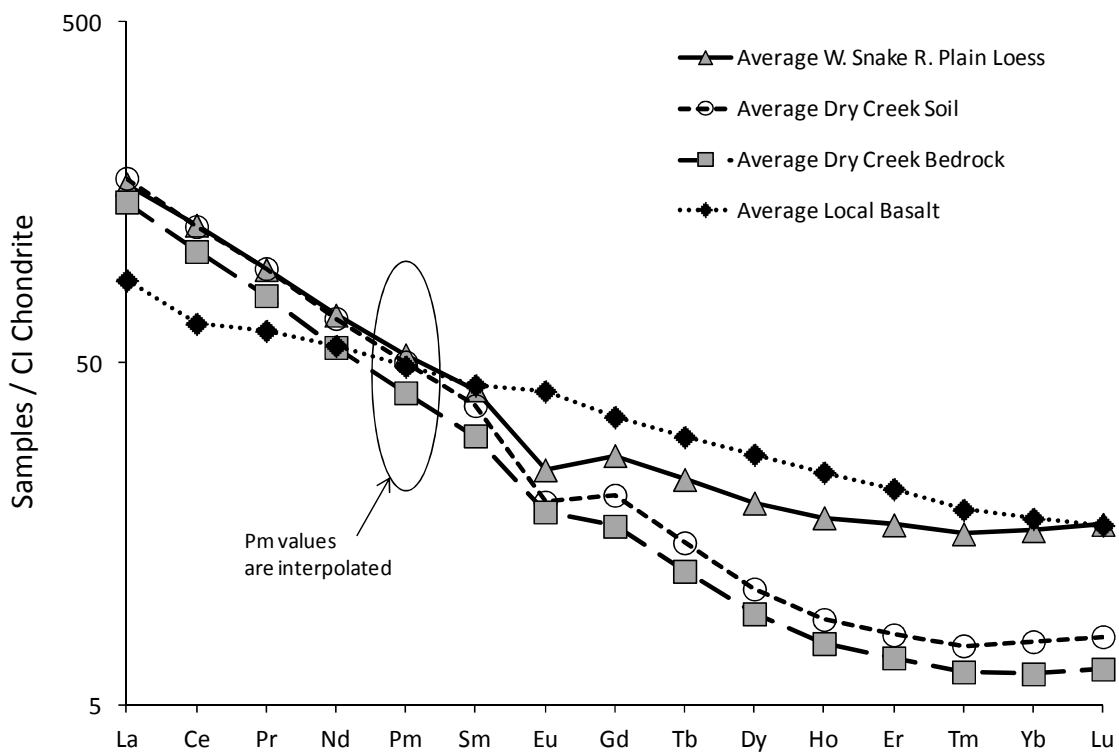


Figure 11: Rare Earth element patterns of DCEW soils, WSRP loess, DCEW bedrock, and local basalt.

Soils, loess, and bedrock exhibit negative Eu anomalies, while basalt shows a slight positive Eu anomaly. Loess and basalt are enriched in the heavy Rare Earth elements relative to soil and bedrock and basalt is depleted in light Rare Earth elements relative to loess, soil, and bedrock. All data is normalized to CI chondrite (McDonough and Sun, 1995).

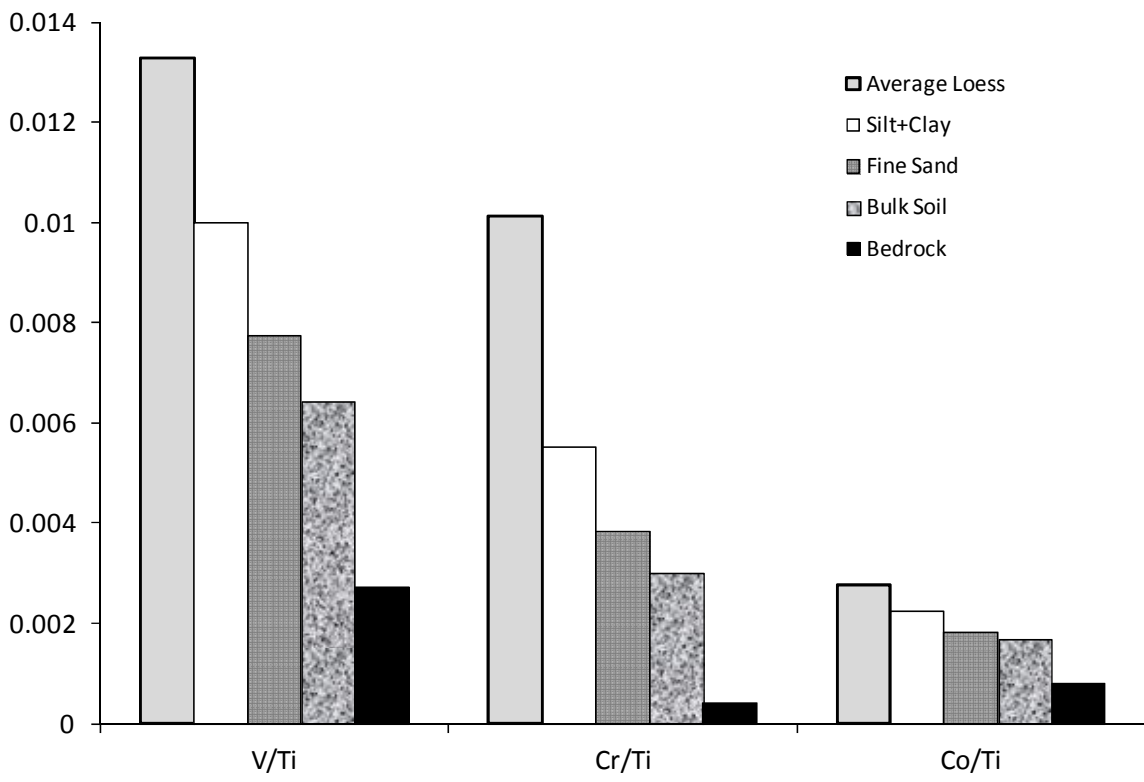


Figure 12: Comparison of trace element concentrations in grain size isolates of selected soil (HS site, 0-10 cm depth).

Bulk soil, silt + clay fraction, and fine sand fraction are shown. Bedrock from the HS site and average loess are included for comparison. The fine sand and silt + clay fractions systematically exhibit concentrations closer to those in the loess population than the bulk soil. Data for the 0-10 cm depth are representative of all other depths at the HS site (20-40 cm and 55-70 cm) so they are not shown here.

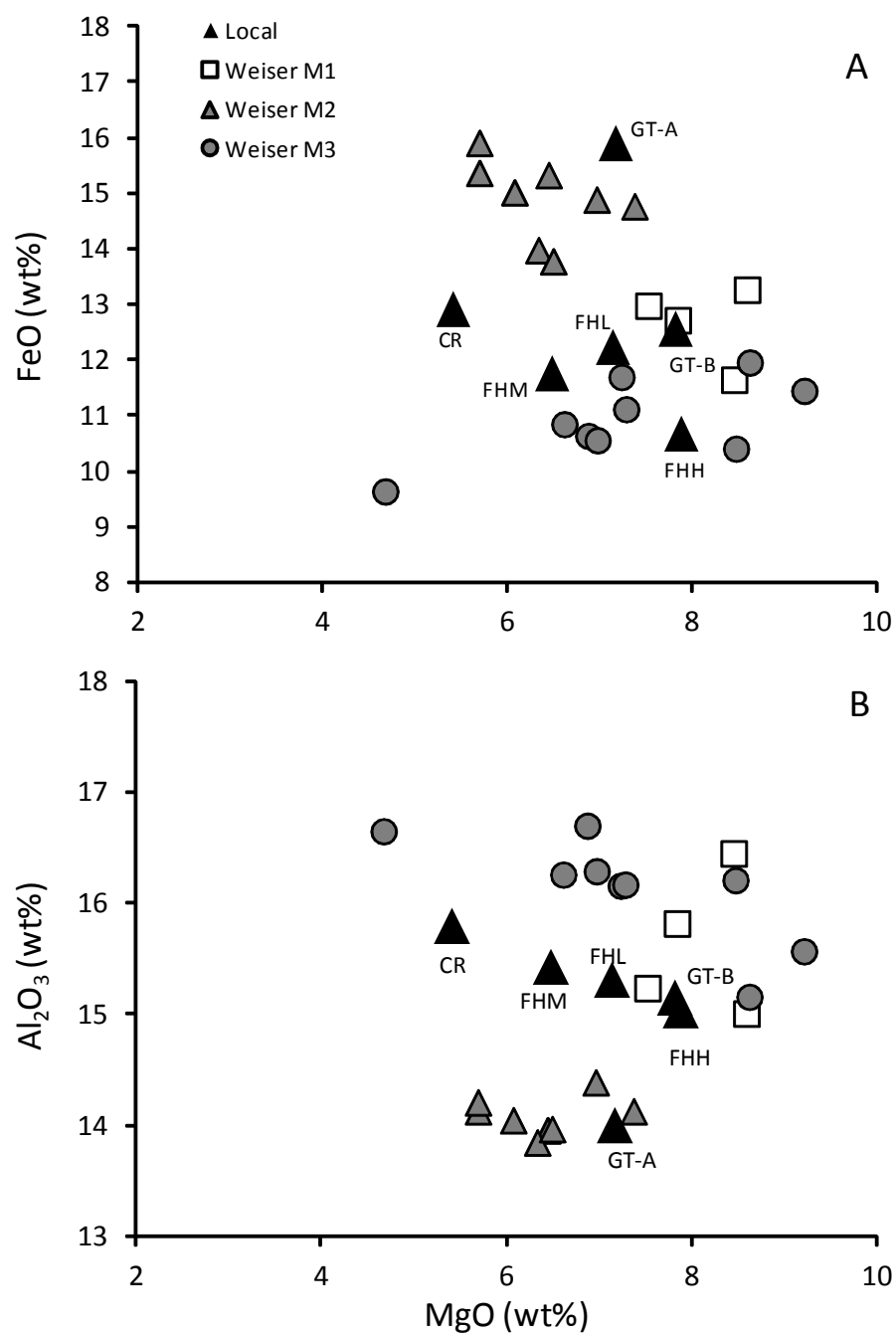


Figure 13: Major element composition of local basalt.

Each of the foothills basalts is labeled individually; Castlerock (CR), Gowen Terrace A (GT-A), Gowen Terrace B (GT-B), Foothills High (FHH), Foothills Middle (FHM) and Foothills Low (FHL). For comparison, data from M1, M2 and M3 type basalts from near Weiser, Idaho (White *et al.*, 2002) is included.

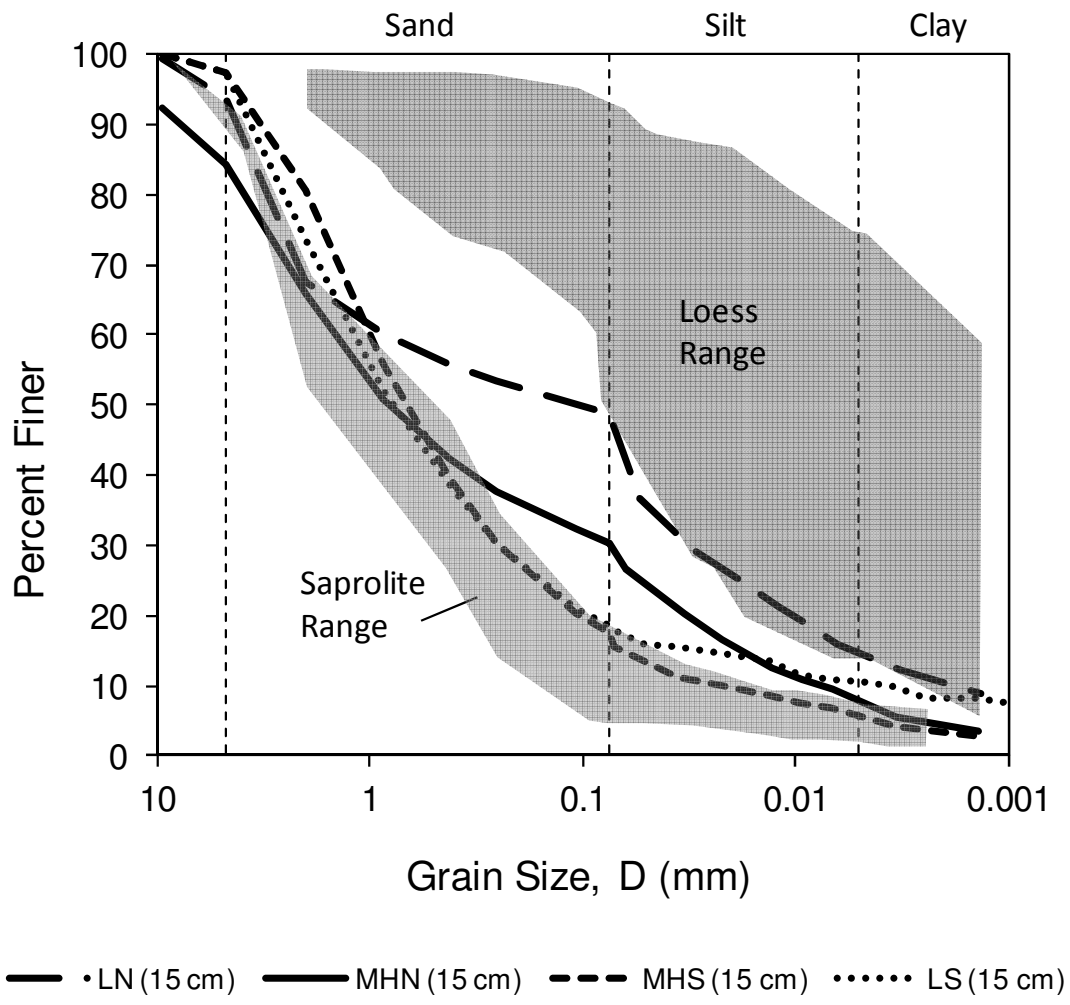


Figure 14: Comparison of grain size distribution curves of saprolites, loess and selected soils.

The shaded areas represent the ranges for saprolite (unpublished data from Riley and Stark, 2010) and loess grain size distribution (unpublished data from Austreng *et al.*, 2010). The black lines show the grain size distribution curves for four shallow soils in the DCEW (data from Smith, 2010).

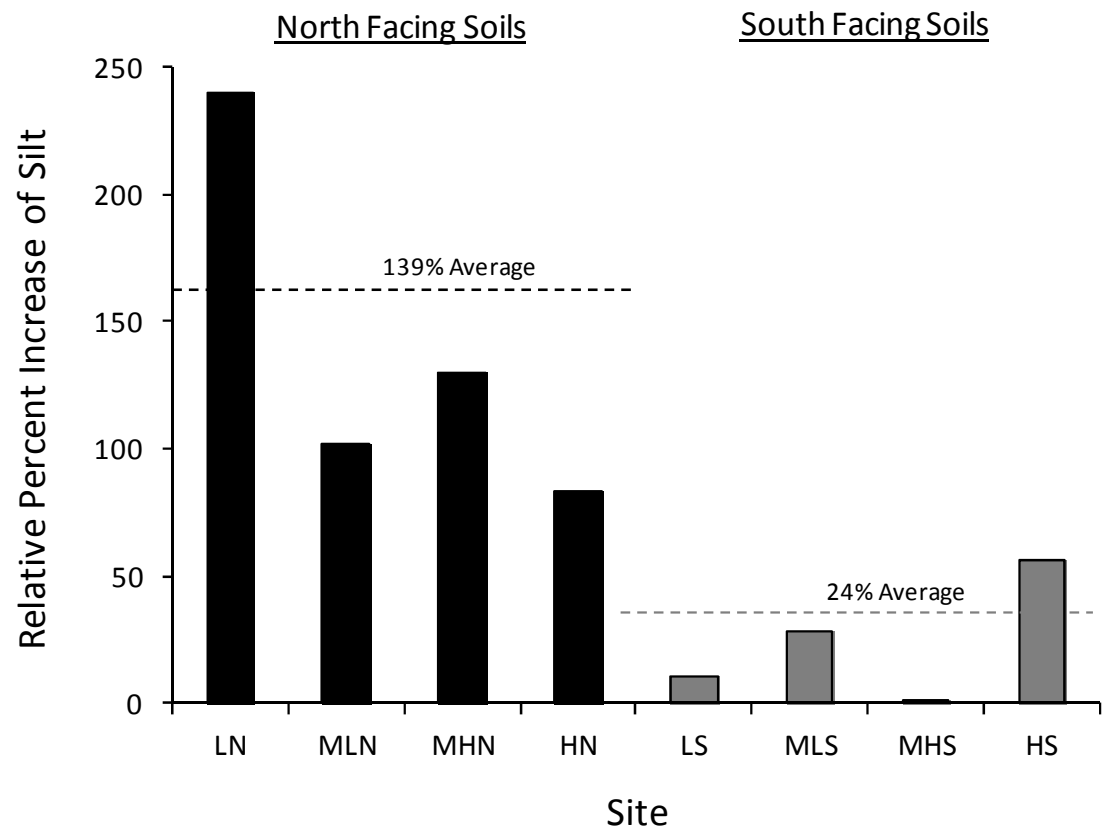


Figure 15: Percent increase in silt content in DCEW soils relative to saprolites.

Site-averaged silt content data from Smith (2010). Silt content data for saprolites from Riley and Stark (2010). Soils on north facing slopes average 139% increase relative to saprolites; soils on south facing slopes average 24% increase relative to saprolites.

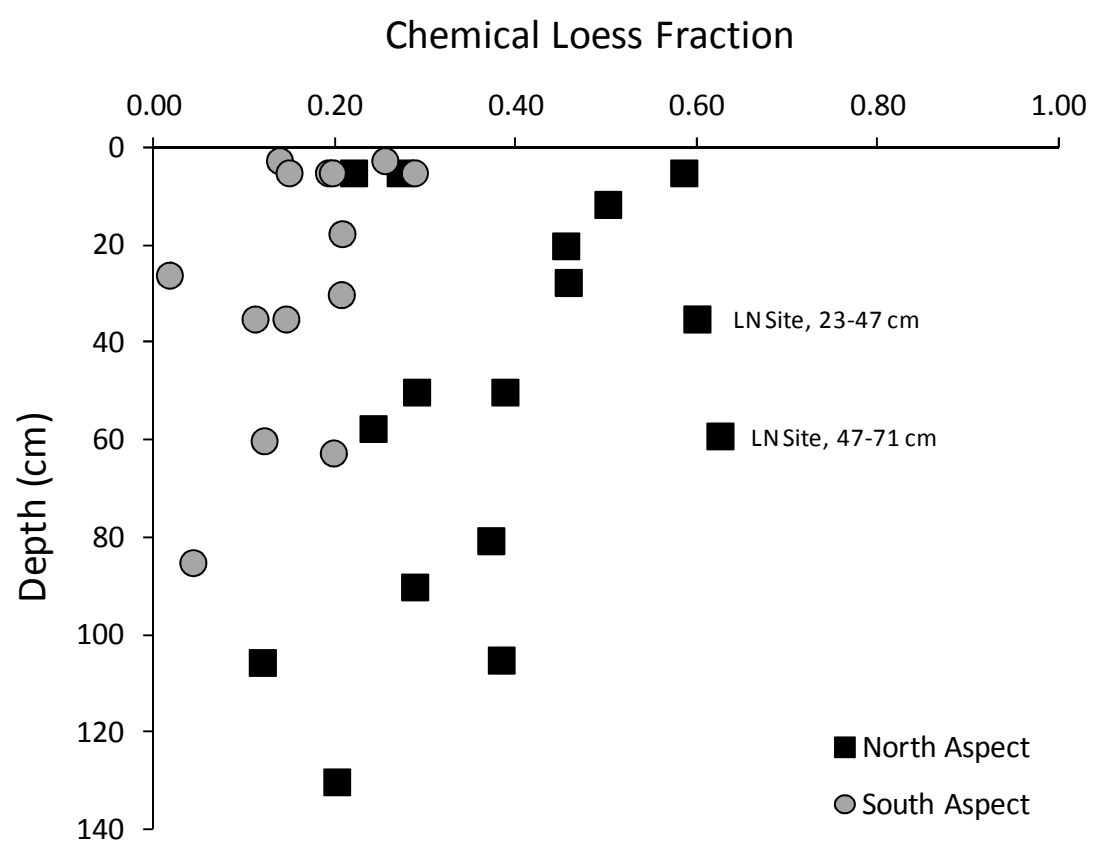


Figure 16: Chemical loess fractions for all soils as a function of soil depth.

The deepest soils within each slope aspect class exhibit lower chemical loess fractions, while the fractions in shallower soils within each are higher. The trend with depth is not strong, but becomes clearer when each slope aspect class is considered independently.

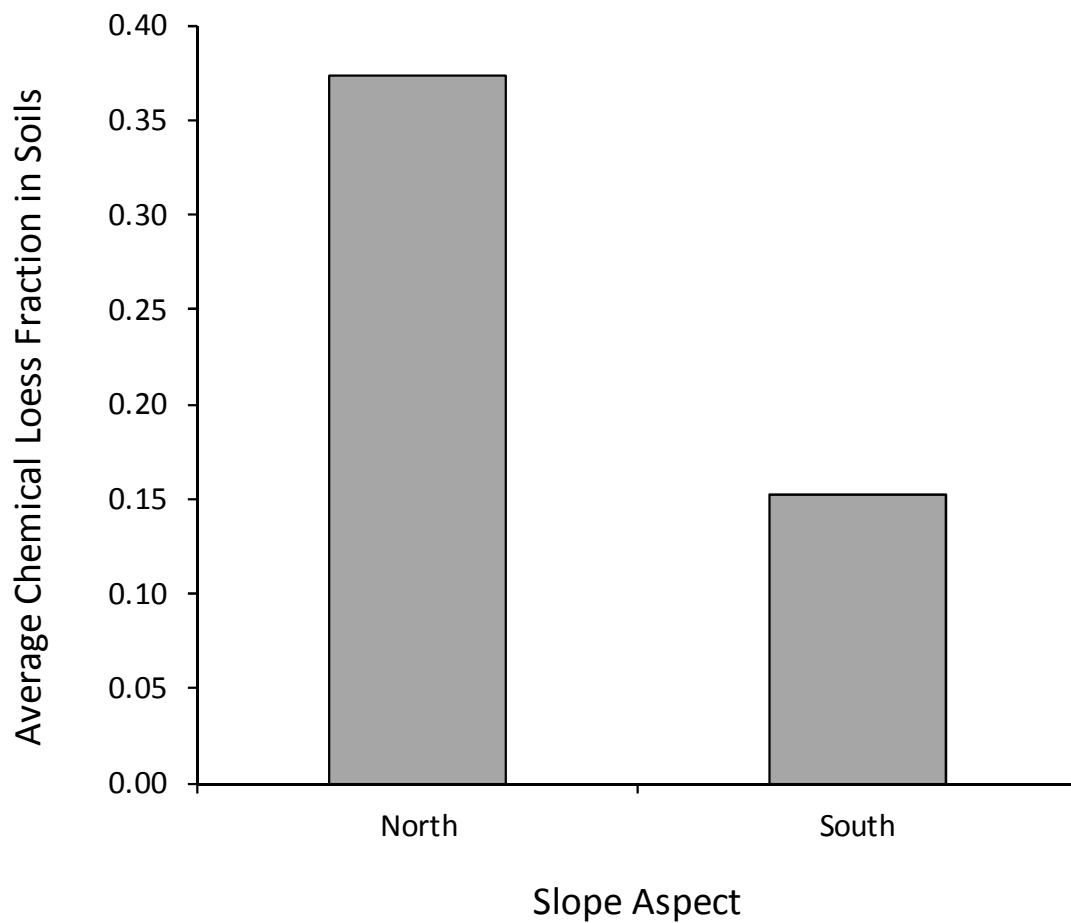


Figure 17: Chemical loess fractions as a function of slope aspect.

North facing soils contain more than twice the average chemical loess fraction of south facing soils (0.38 and 0.16, respectively).

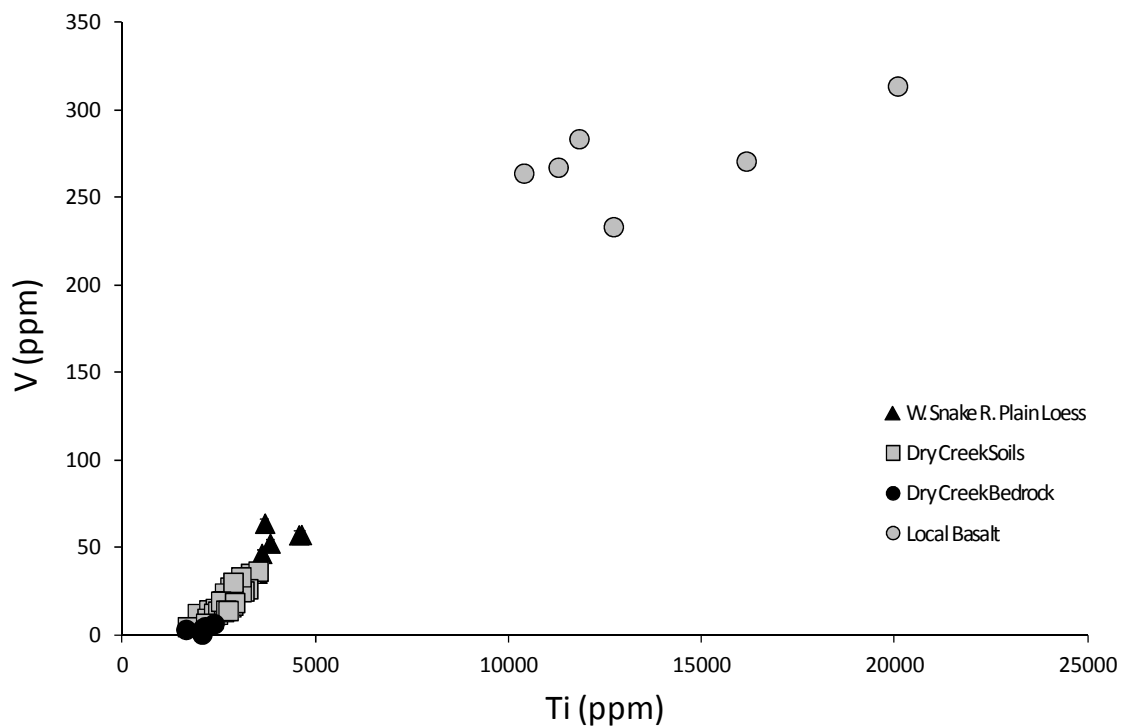


Figure 18: Trace element comparison of local basalt to DCEW bedrock, DCEW soils, and WSRP loess

In V/Ti compositional space, chemical compositions suggest that basalt may be a mixing end-member. Note that the basalt field plots along the same mixing line defined by the bedrock-loess mixing scenario.

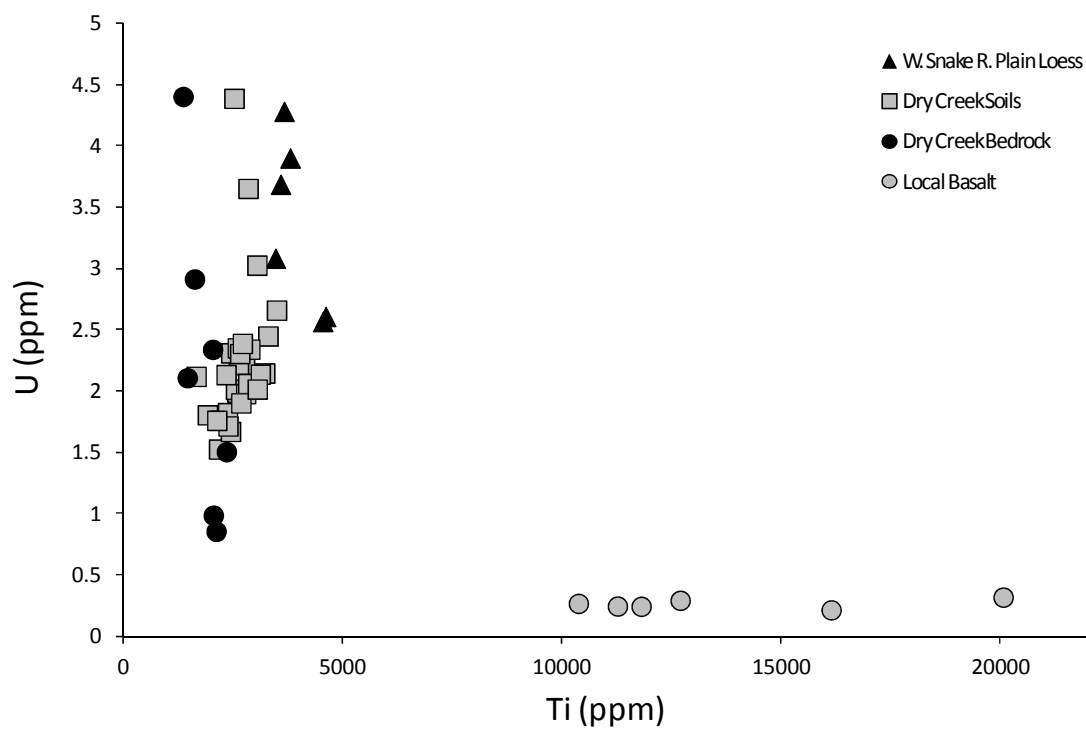


Figure 19: Uranium versus titanium concentrations of local basalt

In U/Ti compositional space, Dry Creek soils appear to be a product of bedrock and loess mixing. U concentrations are very low and Ti concentrations are very high in basalt with respect to bedrock, soils, and loess.

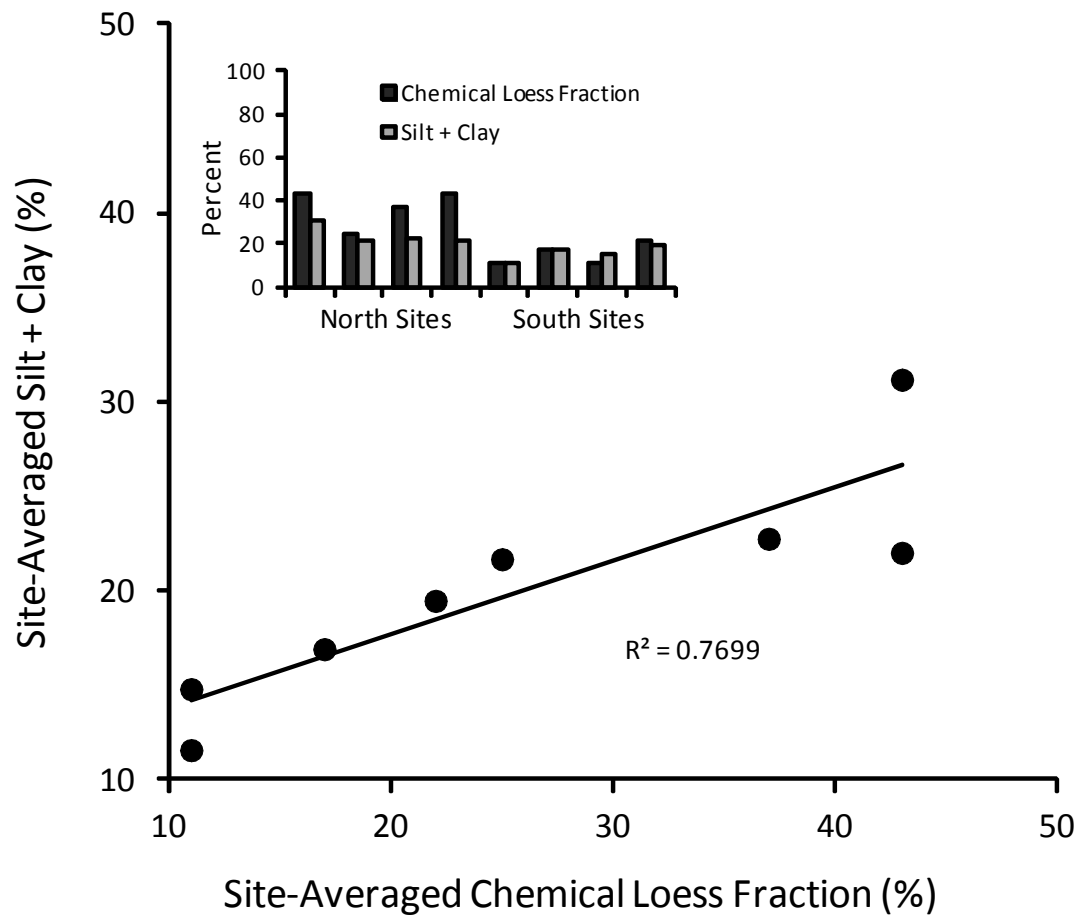


Figure 20: Comparison of chemical loess fractions to existing silt + clay content at Dry Creek soil sites.

Grain size data is from Smith (2010). Chemical loess fraction estimates appear to over-estimate silt content in soils on north facing slopes, but overall there is good correlation to existing grain size data ($R^2 = 0.7699$).

APPENDIX

BSU Isotope Geology Laboratory – Clean Lab Procedures

BSU Isotope Geology Laboratory – Clean Lab Procedures

Sample dissolution (6 x 3 ml PFA bkrs in 125 ml Parr vessel in oven)

1. To each 3 ml Savillex beaker containing the spiked sample, add 0.2 ml conc HNO_3 + 1.8 ml conc HF and swirl to take up all sample powder into a slurry. Place the beakers on a hot plate at 150 °C with the overhead lamp on to dry to a solid sample cake. *This step will begin the reaction and evolution of SiF_4 as a volatile gas.*
2. To each 3 ml Savillex beaker, add 0.2 ml conc HNO_3 + 1.8 ml conc. HF and carefully cap the beaker tightly. Using the special blue tweezers, insert the six 3 ml beakers into the large teflon Parr liner with 7ml of 29M HF “moat” acid. Cap the liner, wrap with parafilm, and remove to the ovens in MG-217. Remove the parafilm from the teflon liner, and slide into the large steel jacket, making sure the bottom plate of the jacket remains loose. Assemble the rest of the jacket cap, and then use the torque wrench to tighten down the cap screws in an alternating star pattern. Place the assembled jacket into the 220 °C oven for 48 hours.
3. Remove Parr vessels from oven, cool, remove the liner from the jacket and wipe down thoroughly. The liner should still be sealed--bring into clean lab. In the clean lab, loosen Parr vessel cover by tapping around edge with a spare liner, then use a square of Parafilm to twist open, breaking the seal.
4. Remove the six 3 ml beakers from the Parr liner with the special blue tweezers, keeping them horizontal, then rinse the outsides with MQ-H₂O and dry with a DurX wiper. Uncap each beaker and place on the hotplate.
5. Add 0.5 ml conc HNO₃ to each beaker, and dry @ 120 °C under lamp to a dry sample cake. **Repeat this process two more times.**
6. To each 3 ml Savillex beaker, add 2 ml 6M HCl and carefully cap the beaker tightly. Using the special blue tweezers, insert the six 3 ml beakers into the large teflon Parr liner with 7ml of 6M HCl “moat” acid. Cap the liner, wrap with parafilm, and remove to the ovens in MG-217. Remove the parafilm from the teflon liner, and slide into the large steel jacket, making sure the bottom plate of the jacket remains loose. Assemble the rest of the jacket cap, and then use the torque wrench to tighten down the cap screws in an alternating star pattern. Place the assembled jacket into the 180 °C oven for 12 hours.
7. Remove Parr vessels from oven, cool, remove the liner from the jacket and wipe down thoroughly. The liner should still be sealed--bring into clean lab. In the clean lab, loosen Parr vessel cover by tapping around

edge with a spare liner, then use a square of Parafilm to twist open, breaking the seal.

8. Remove the six 3 ml beakers from the Parr liner with the special blue tweezers, keeping them horizontal, then rinse the outsides with MQ-H₂O and dry with a DurX wiper. Uncap each beaker and visually inspect – you should have a clear (though likely colored) solution with no visible solids. Pour the contents into a 15 ml Savillex beaker for subsequent column chemistry preparation. Start cleaning the 3 ml beakers immediately (conc HF + HNO₃ overnight, 6M HCl overnight).